Freezing of $HNO_3/H_2SO_4/H_2O$ Solutions at Stratospheric Temperatures: Nucleation Statistics and Experiments

Thomas Koop,* Beiping Luo, Uta M. Biermann, Paul J. Crutzen, and Thomas Peter

Max Planck Institute for Chemistry, Postfach 3060, 55020 Mainz, Germany

Received: August 30, 1996; In Final Form: November 6, 1996[⊗]

Calorimetric freezing experiments with aqueous sulfuric and nitric acid solutions are presented and applied to the formation of polar stratospheric clouds (PSCs). We show that the nucleation of hydrates from these solutions is a stochastic process and that nucleation rates and their uncertainties can be determined using Poisson statistics. Under thermodynamic equilibrium conditions above the ice frost point, the homogeneous nucleation rates of stratospheric aerosols are exceedingly low, ruling out homogeneous freezing as a pathway for PSC formation. Several stratospherically important substrates were tested concerning their ability to induce heterogeneous nucleation. None of the experiments indicated a relevant enhancement of the freezing probability of liquid aerosols. Moreover, the experiments reveal that the freezing process of the solutions under stratospheric conditions is limited by the nucleation rates of the hydrates, rather than their crystal growth rates, thus ruling out the possibility of a glassy state of stratospheric aerosol droplets. Also, we argue why a glacial state of the aerosols seems to be unlikely. The only processes leading to freezing of the hydrates appear to be the heterogeneous nucleation on water ice crystals forming below the frost point and the homogeneous freezing of almost binary HNO_3/H_2O droplets with H_2SO_4 concentrations below approximately 0.01 wt %.

1. Introduction

There is growing observational evidence[1−3] based on remote sensing[4,5] and *in situ* measurements[6,7] that stratospheric sulfuric acid aerosols may remain liquid to the lowest polar winter temperatures despite a considerable supersaturation (≈30) with respect to the hydrates of sulfuric and nitric acid. The liquid state of the aerosol falsifies the conventional three-stage concept[8] of (1) having frozen H_2SO_4/H_2O aerosol particles at temperatures above 195 K, (2) the formation of nitric acid trihydrate[9−11] (NAT, $HNO_3 \cdot 3H_2O$) at $T \lesssim 195$ K on the largest H_2SO_4/H_2O particles due to sublimative nucleation, and (3) the formation of water ice at temperatures below the frost point ($T \lesssim 188$ K) on the largest NAT particles, again due to sublimative nucleation.

On the other hand, field measurements show the widespread occurrence of crystalline polar stratospheric clouds (PSCs) above the frost point.[12−14] At present there are several theories of how solid PSCs form. Early studies suggested that NAT would form in stratospheric droplets due to the uptake of HNO_3 which is more soluble at low temperatures.[15,16] Also different metastable hydrates have been observed in laboratory measurements and have been proposed to form in the first place instead of the thermodynamic stable NAT: nitric acid dihydrate[17] (NAD, $HNO_3 \cdot 2H_2O$), nitric acid pentahydrate[18] (NAP, $HNO_3 \cdot 5H_2O$), and a mixed hydrate[19] $HNO_3 \cdot H_2SO_4 \cdot 5H_2O$ (MIX). Recently, some field measurements have been interpreted in terms of nitric acid decahydrate or even higher hydrates.[20] In contrast, on the basis of bulk freezing experiments it has been argued that homogeneous freezing of ternary liquid aerosols under equilibrium conditions can only occur below the frost point.[21] Other theories involve the formation of amorphous solid solutions with glasslike properties which crystallize upon warming[22] or the homogeneous freezing in droplets whose concentrations are highly perturbed from equilibrium due to strong temperature fluctuations in lee waves.[23]

The consequences of the uncertainties in our microphysical understanding of the aerosol for the chemical modeling of the stratosphere are not yet fully clear. It has been argued that the chemical reaction probabilities of chlorine compounds on liquid surfaces as compared to solid hydrate surfaces are of similar magnitude.[24] However, liquid particles may show even higher reaction probabilities[25,26] and develop different volumes and surface areas[1] compared to solid particles at the same temperature, possibly leading to large differences in chemical chlorine processing. The complicated processes of coupled gas and liquid phase diffusion, interfacial mass transfer, and liquid phase reactivity have been described in a satisfactory fashion.[27] On the other hand, a full comparative modeling of liquid and solid chemical processing is still hampered by our lack of knowledge of the two principal nucleation mechanisms—sublimative nucleation on solid nuclei and freezing of hydrates from binary or ternary liquid aerosols. While there is only limited quantitative information on sublimative nucleation rates,[16,28] a number of laboratory experiments have been undertaken to investigate freezing nucleation using liquid bulk samples[15,21,29−32] or droplet ensembles[33−35] in order to estimate the freezing rates. A sound theoretical interpretation of the experiments is lacking, and too high freezing rates have been erroneously deduced for HNO_3-rich solutions, for which only Koop *et al.*[21] demonstrated their negligible freezing probability.

In this work we present new experimental data for freezing rates of sulfuric and nitric acid hydrates from binary and ternary bulk solutions together with a theoretical derivation of the statistics of the nucleation process which allows the evaluation of both bulk phase and aerosol freezing experiments in a self-consistent way. We show that a careful setup of the experiments is needed, in particular to avoid the formation of frost or nitric acid hydrates on the containment walls which inevitably falsifies the results. The new data, in combination with data from the existing literature, are used to calculate upper bounds for the rates of homogeneous nucleation of the various hydrates. From this, we corroborate our earlier findings that the hydrates under thermodynamic equilibrium conditions are very unlikely to nucleate homogeneously in stratospheric aerosol droplets above the frost point.[21] Even heterogeneous nucleation of the hydrates

[⊗] Abstract published in *Advance ACS Abstracts,* January 1, 1997.

S1089-5639(96)02653-9 CCC: $14.00

appears to be unlikely unless the stratospheric aerosols contain nuclei many orders of magnitude more effective than the glass walls of the experimental setup and the nuclei in the unfiltered acidic solutions. In addition, we show that a glacial (solid amorphous) or glassy state of stratospheric aerosols is very unlikely.

Applied to the stratosphere this means that aerosol particles under equilibrium conditions freeze only below the frost point and that the formed ice crystals may serve as nuclei for the formation of nitric acid hydrates and/or sulfuric acid hydrates. Alternatively, a possible freezing mechanism above the frost point is the formation of almost binary HNO_3/H_2O droplets with very little H_2SO_4, but this requires high cooling rates as they occur in the atmosphere only in orographically strongly perturbed regions. At present neither the microphysical nor the meteorological conditions under which such a mechanism works are fully understood.

2. Theoretical Section

I. Statistics of the Nucleation Process. We first investigate the case where the crystallization of a sample after nucleation is much faster than the nucleation process itself. In section 2.IV we generalize the description for cases with slow crystallization. For stratospherically relevant systems the crystallization time is usually so short that it can be neglected, as shown in section 2.V.

Nucleation is a stochastic process, similar to radioactive decay. This means that the formation of a critical embryo, i.e. a successful nucleation act, does not depend on the number of trials that have taken place previously, and that different nucleation acts are independent of each other.

Consider an ensemble of m molecules each of which has a probability p to become the center of a critical nucleus during a certain observation time. Then the probability to observe k nucleation acts, $P_k(m)$, is given by the binomial distribution

$$P_k(m) = \frac{m!}{k!(m-k)!} p^k (1-p)^{m-k} \tag{1}$$

In a bulk sample of 1 cm^3, m is usually of the order of 10^{22}, and even in a 1 μm droplet m is still about 10^{10}. For large m, but small p and hence a very small molecular nucleation probability, eq 1 simplifies with the help of Stirling's formula (see Appendix 1) and yields the Poisson distribution

$$P_k(m) \simeq \frac{(mp)^k}{k!} e^{-mp} \tag{2}$$

When the probability p for a single molecule is sufficiently small ($p \ll 1$), it simply increases linearly[36] with observation time ($p \propto t$). Therefore, we define a constant rate $\omega \equiv mp/t$, which is the nucleation rate of the whole sample (in s^{-1}), while t is time (in s) and p/t is the nucleation rate for a single molecule in the sample. We obtain the Poisson distribution for nucleation

$$P_k(t) = \frac{(\omega t)^k}{k!} e^{-\omega t} \tag{3}$$

The function $P_k(t)$ is the probability for observing exactly k incidences of nucleation within the time interval $[0,t]$. In particular, for $k = 0$, which means that no nucleation occurs as time progresses, it is

$$P_0(t) = e^{-\omega t} \tag{4}$$

which is the well-known exponential decay law (similar to radioactive decay). $P_0(t)$ can be regarded as the probability that a sample is still liquid after time t, because no nucleation has occurred.

The exponential decay is also revealed by assuming that nucleation is a first-order reaction.[37,38] However, this approach refers to a large ensemble of identical samples or a large number of repeated experiments with one sample, while we used a molecular description which allows derivation of an upper bound for the nucleation rate coefficient also when only a single experiment with one sample has been performed.

To apply Poisson statistics to the freezing process, it should be noted that after the first nucleation act usually the entire sample rapidly crystallizes and the measurement has to be stopped. To obtain statistical information, the same experiment must be repeated several times (while resetting the time to zero for each trial), or alternatively several equal samples must be used simultaneously. We now consider n_{tot} equal samples, e.g. test tubes or aerosol droplets, each containing enough molecules m so that eq 2 applies. The probability that n_{liq} samples do not nucleate within an observation time t is given by

$$P_0(t) = e^{-\omega t} \simeq \frac{n_{liq}(t)}{n_{tot}} \tag{5}$$

Hence, the number of nucleation events as a function of time should follow an exponential curve. The approximation in eq 5 becomes more accurate as the number of samples n_{tot} is increased, but even for rather small n_{tot} ($\gtrsim$5), the slope of the exponential can be used to calculate the nucleation rate ω. The other Poisson functions P_k ($k \geq 1$) for the probability of observing k nucleation events within a specific time interval can be related to experimental data by

$$P_k(t) = \frac{(\omega t)^k}{k!} e^{-\omega t} \simeq \frac{n_{liq}(t)}{n_{tot} k!} \left(\ln\left\{ \frac{n_{tot}}{n_{liq}(t)} \right\} \right)^k \tag{6}$$

The properties of Poisson statistics can be used to determine the nucleation rate from experiments in the following manner: If in an experiment n_{nuc} samples nucleate after times $t_{nuc,i}$ ($i = 0 \ldots n_{nuc}$) and n_{liq} samples remain liquid over times $t_{liq,i}$ ($i = 0 \ldots n_{liq}$), the total observation time is

$$t_{tot} = \sum_{i=0}^{n_{liq}} t_{liq,i} + \sum_{i=0}^{n_{nuc}} t_{nuc,i} \tag{7}$$

and the nucleation rate may be obtained from

$$n_{nuc} = \sum_{k=0}^{\infty} k P_k(t_{tot}) = \sum_{k=1}^{\infty} k \frac{(\omega t_{tot})^k}{k!} e^{-\omega t_{tot}} = \omega t_{tot} \sum_{k=1}^{\infty} \frac{(\omega t_{tot})^{k-1}}{(k-1)!} e^{-\omega t_{tot}} = \omega t_{tot} \sum_{k'=0}^{\infty} \frac{(\omega t_{tot})^{k'}}{(k')!} e^{-\omega t_{tot}} = \omega t_{tot} \sum_{k'=0}^{\infty} P_{k'}(t_{tot}) = \omega t_{tot} \tag{8}$$

where $k' = k - 1$ and the normalization $\sum_{k'=0}^{\infty} P_{k'}(t_{tot}) = 1$ was used. Thus,

$$\omega = \frac{n_{nuc}}{t_{tot}} \tag{9}$$

If n_{nuc} is the expectation value for the number of nucleation events, eq 9 yields the most likely value for ω under arbitrary

experimental conditions. However, also for higher or lower values of ω the probability for n_{nuc} nucleation events to occur within t_{tot} is greater than zero. This can be used to derive a statistical uncertainty in ω for a given number of detected events on a fixed confidence level x. The lower fiducial limit, ω_{low}, is defined such that less than n_{nuc} nucleation events would occur with a probability x if ω_{low} were the true nucleation rate:[39]

$$x = \sum_{k=0}^{n_{nuc}-1} P_k(t_{tot}) = e^{-\omega_{low}t_{tot}} \sum_{k=0}^{n_{nuc}-1} \frac{(\omega_{low}t_{tot})^k}{k!} \quad (10a)$$

Correspondingly for the upper fiducial limit, ω_{up}:

$$x = \sum_{k=n_{nuc}+1}^{\infty} P_k(t_{tot}) = 1 - e^{-\omega_{up}t_{tot}} \sum_{k=0}^{n_{nuc}} \frac{(\omega_{up}t_{tot})^k}{k!} \quad (10b)$$

The probability x is also called "confidence level", i.e. the probability for $\omega > \omega_{low}$ (eq 10a) and $\omega < \omega_{up}$ (eq 10b). Note that the probability for $\omega_{low} < \omega < \omega_{up}$ is $p = 1 - 2(1 - x)$. Even if no single nucleation event occurs ($n_{nuc} = 0$), eq 10b allows an upper fiducial limit for ω to be determined

$$\omega_{up} = \frac{1}{t_{tot}} \ln\left(\frac{1}{1-x}\right) \quad (11)$$

We applied this equation in our earlier work[21] to calculate upper fiducial limits for the homogeneous nucleation rates of ternary solutions. Typical values for upper and lower fiducial limits for different numbers of freezing events on a confidence level $x = 0.999$ are given in Table 2 in Appendix 2.

For large numbers of nucleation events ($n_{nuc} \gtrsim 100$), as for example in aerosol chamber experiments evaluation of eqs 10a,b becomes cumbersome but can be facilitated by reducing the binomial distribution of eq 1 to the normal distribution (see Appendix 1)

$$P_k(m) \simeq \frac{1}{\sigma(2\pi)^{1/2}} \exp\left(-\frac{(k-mp)^2}{2\sigma^2}\right) \quad (12)$$

with $\sigma^2 = mp(1 - p)$. As long as the expectation value $n_{nuc} \simeq mp \ll m$, σ can be approximated by $\sigma^2 \simeq n_{nuc}$. The lower and upper fiducial limits for ω are then (Appendix 2)

$$\omega_{low} = \frac{1}{t_{tot}}(n_{nuc} - [1 + (2n_{nuc})^{1/2}\,\mathrm{erf}^{-1}(2x-1)]) \quad (13a)$$

$$\omega_{up} = \frac{1}{t_{tot}}(n_{nuc} + [1 + (2n_{nuc})^{1/2}\,\mathrm{erf}^{-1}(2x-1)]) \quad (13b)$$

where erf^{-1} is the inverse error function (see Table 4).

A typical application for the normal distribution fiducial limits are aerosol chamber experiments with FTIR-spectroscopy for the detection of freezing.[33−35] For example, if $n_{nuc} = 3 \times 10^5$ out of $n_{tot} = 10^6$ particles are detected to have nucleated after a certain observation time, the statistical uncertainty in the number of nucleation events on a confidence level $x = 0.999$ can be calculated from the term in square brackets in eqs 13a,b: $[1 + (2n_{nuc})^{1/2}\,\mathrm{erf}^{-1}(2x-1)] \simeq 1694$. Hence, the relative statistical uncertainty is $1694/(3 \times 10^5) \simeq 0.6\%$, which is much smaller than the typical measurement uncertainty for the detection of the frozen fraction in FTIR experiments (usually ≈5%). Therefore the statistical uncertainty can be neglected in this particular case.

II. Nucleation Rate Coefficients. Next, we examine the underlying physical quantities that can be retrieved from the measured rate ω (in s^{-1}). Often, several competing nucleation processes exist simultaneously in one sample. For instance, the sample might be supercooled with respect to different solid phases, or both homogeneous and heterogeneous nucleation are possible, or there are several heterogeneous processes when the solution is in contact with substrates of different surface properties. Since the corresponding processes are independent of each other, the total probability that no nucleation occurs, $P_{0,tot}(t)$, is the product of the probabilities that none of the individual processes induces nucleation

$$P_{0,tot}(t) = P_{0,1}(t)P_{0,2}(t) \ldots P_{0,n}(t) \quad (14)$$

Rearranging eq 14 with the help of eq 4 leads to

$$P_{0,tot}(t) = e^{-\omega_{tot}t} = e^{-\omega_1 t}\, e^{-\omega_2 t} \ldots e^{-\omega_n t} = e^{-(\omega_1+\omega_2+\ldots+\omega_n)t} \quad (15)$$

so that

$$\omega_{tot} = \omega_1 + \omega_2 + \ldots + \omega_n \quad (16)$$

For instance, the experimentally determined rate ω for a sample of volume V in contact with two substrates with surface areas A_1 and A_2 supercooled with respect to a single solid phase is given by

$$\omega = \omega_{hom} + \omega_{het,1} + \omega_{het,2} = JV + j_1A_1 + j_2A_2 \quad (17)$$

where $J = J(T, c)$ (in $cm^{-3}\ s^{-1}$) and $j_i = j_i(T, c)$ (in $cm^{-2}\ s^{-1}$) are the temperature (T) and concentration (c) dependent homogeneous and heterogeneous nucleation rate coefficients, respectively. While it is often difficult to separate these processes experimentally, the determined ω always constitutes an upper bound for each individual rate coefficient. Also, often one of the rate coefficients is much greater than the others, and then dominates the total nucleation rate coefficient.

It should be noted that up to here experimental conditions like temperature and concentrations were assumed to be constant (i.e. ω is time independent). Since P_0 in eq 5 satisfies the differential equation[37,38]

$$\frac{dP_0}{dt}(t) = -\omega P_0(t) \quad (18a)$$

a generalization for time-dependent parameters is given by

$$\frac{n_{liq}(t)}{n_{tot}} \simeq P_0(t) = \exp(-\int_0^t \omega(T(t),c(t))\,dt) \quad (18b)$$

From eq 18b, in principle, the nucleation rate for a range of parameters may be retrieved. However, the unfolding of the integral requires many measurements, so that it is usually more feasible to cool the sample to the desired temperature and then to keep it constant. Time zero then is the point when the sample reaches the desired temperature (and not at the beginning of the cooling).

III. Statistically Inhomogeneous Ensembles. The formalism provided in section 2.I assumes that each of the samples is subject to the same mechanisms causing the nucleation. This is true, if they all have the same temperature, volumes, and concentrations and are exposed to the same solution impurities and heterogeneous surfaces. However, in a real experiment this is not always the case. Different test tubes can behave very differently concerning heterogeneous nucleation due to the presence of active sites on the glass, e.g. in the vicinity of a scratch. As we will show below, the presence of different

nucleation processes is often suggested when a subset of the samples freezes much more rapidly than the others. Theoretically this can be described as follows. We assume that all samples are subject to a slow nucleation process with a rate ω_{slow}. In addition, a fraction α of the samples is subject to a second nucleation process with a rate ω_2 leading to an overall rate $\omega_{fast} = \omega_{slow} + \omega_2$. Hence, the freezing probability $P_0(t)$ of all the samples can be expressed as the sum of two exponentials weighted by α:

$$P_0(t) = \alpha e^{-\omega_{fast}t} + (1 - \alpha)e^{-\omega_{slow}t} \tag{19}$$

The additional nucleation process is an experimental artifact (e.g. from not using identical tubes). If such an artifact occurs, following the formalism of Poisson statistics as described above would overestimate the upper bounds for the individual homogeneous and heterogeneous nucleation rate coefficients. This is because the upper bound is then not determined by ω_{slow} as would be correct, but by

$$\omega_{tot} = \frac{n_{nuc,fast} + n_{nuc,slow}}{t_{tot}} = \frac{-\ln(\alpha e^{-\omega_{fast}t_{tot}} + (1 - \alpha)e^{-\omega_{slow}t_{tot}})}{t_{tot}} \tag{20a}$$

with

$$\omega_{fast} = \frac{n_{nuc,fast}}{t_{fast}} \qquad \omega_{slow} = \frac{n_{nuc,slow}}{t_{slow}} \tag{20b}$$

where t_{fast} and t_{slow} are defined similar to eq 7. Equation 20a reduces to $\omega_{tot} = \omega_{fast}$ when the additional process is present in all samples ($\alpha = 1$) and to $\omega_{tot} = \omega_{slow}$ in the absence of experimental artifacts ($\alpha = 0$). It is clear that the additional process must be a heterogeneous nucleation process, because homogeneous nucleation is possible in all the samples. Whenever feasible, an evaluation of freezing experiments should be performed according to eqs 19 and 20b instead of the averaging procedure in eq 20a. Examples follow below (see Figures 8 and 9).

IV. Nucleation and Crystallization. Nucleation measurements are complicated by the fact that nucleation does not necessarily lead to instantaneous freezing of the sample. For example, calorimetric freezing experiments rely on the release of latent heat which is monitored as an indicator of the formation of a more stable phase. Nucleation leads merely to the formation of a stable germ and even after some time the growing germ is still so small in size that the latent heat release is too small to be detected. Only after the germ has grown to a size large enough to increase the temperature of the entire sample, freezing and therefore nucleation become detectable. Therefore, the measured freezing time t_{fr} is the sum of the time the sample needs to nucleate, t_{nuc}, and the time the germ needs to grow to an appropriate size, t_{cryst}:

$$t_{fr} = t_{nuc} + t_{cryst} \tag{21}$$

The crystal growth time, t_{cryst}, depends on the stoichiometry of the growing crystal, on the concentration, supercooling, and viscosity of the liquid solution under the experimental conditions, and on the method used to detect the germ. For example, the crystal growth of the sulfuric acid tetrahydrate (SAT, $H_2SO_4 \cdot 4H_2O$) is very rapid from a solution with a stoichiometry of $H_2SO_4:H_2O = 1:4$ ($\approx$57.6 wt %), while it is much slower in a solution of 1:6.5 ($\approx$45.6 wt %) at the same temperature despite the lower viscosity of the latter solution. On the other hand, in the 1:6.5 solution the crystal growth of the sulfuric acid hemihexahydrate (SAH, $H_2SO_4 \cdot 6.5H_2O$) is very fast as can be seen in Figure 1. Usually, the larger the difference in concentration between the crystallizing hydrate and the solution, the slower the crystal growth. The reason is that the limiting step for a solution with the ideal stoichiometry is merely the reorientation of the molecules to be integrated into the crystal lattice and the diffusion of heat, while in a solution with nonideal stoichiometry a diffusive flux has to maintain the necessary molecular transport to the growing crystal. Furthermore, the degree of supercooling plays a role as it is the driving force for the crystal growth. In Figure 1 the 1:4 solution at 191 K is supercooled by 53 K with respect to SAT, while SAH in a 1:6.5 solution is supercooled only by 25 K, leading to a faster crystal growth of SAT. In the light of these considerations we can modify eq 9 to take account of the finite crystallization time. For simplicity we treat only the case that all samples freeze ($t_{tot} = \sum_i^{n_{nuc}} t_{nuc,i}$ in eq 7):

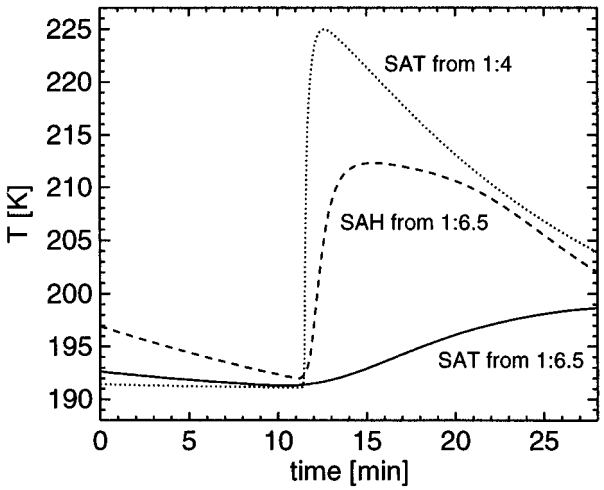

Figure 1. Sample temperature during crystallization for different H_2SO_4/H_2O solutions at stratospheric temperatures. Samples of 2 cm^3 volume in a glass tube were insulated by foam from the environment. Three different experiments are shown: solid line, SAT crystallizing from a 1:6.5 solution; dashed line, SAH crystallizing from a 1:6.5 solution; dotted line, SAT crystallizing from a 1:4 solution. The nature of the crystallizing solid was checked afterward by determining the melting points in each case (SAT/ice-eutectic, 200 K; SAH, 220 K; SAT, 245 K).

$$\omega_{nuc} = \frac{n_{nuc}}{\sum_i t_{nuc,i}} = \frac{n_{nuc}}{\sum_i t_{obs,i} - n_{nuc}t_{cryst}} = \left(\frac{1}{\omega_{obs}} - \frac{1}{\omega_{cryst}}\right)^{-1} \tag{22}$$

Here, ω_{nuc} is the statistically averaged nucleation rate ($\omega_{nuc} = JV$ for homogeneous nucleation or $\omega_{nuc} = jA$ for heterogeneous nucleation), ω_{obs} is the observed freezing rate with $t_{obs,i} = t_{nuc,i} + t_{cryst}$, and $\omega_{cryst} = t_{cryst}^{-1}$ is the inverse of the crystal growth time (which depends on the sensitivity of the device used to detect the germ). The crystal growth time leads to a systematic offset of the freezing times, and eq 5 is not obeyed when assuming $\omega = \omega_{obs}$. Hence, if in a freezing experiment ω_{cryst} is much smaller than ω_{nuc}, it is not possible to measure the nucleation rate. In this case the freezing process depends entirely on the growth habit of the crystal, whose details are usually not sufficiently well-known to obtain reliable information on J. Then, instead of using a simple calorimetric device (see Figure 5 below), more sensitive techniques like differential scanning calorimetry or optical detection of the germs may be used in order to increase the ratio of $\omega_{cryst}/\omega_{nuc}$. Surprisingly

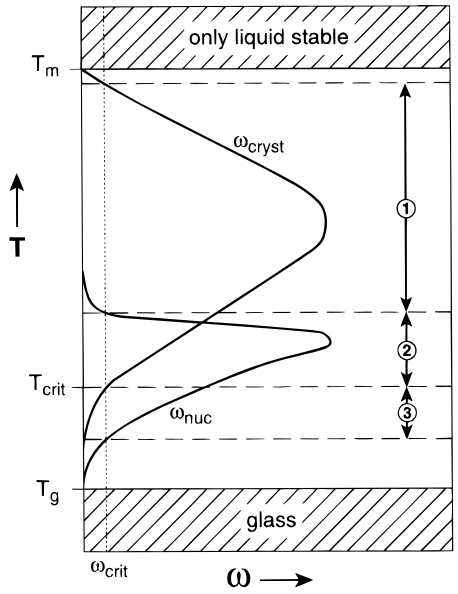

Figure 2. Schematic plot of the temperature dependence of the nucleation rate, ω_{nuc}, and the crystal growth rate, ω_{cryst}, for a solution of given composition and volume in the investigated binary and ternary $HNO_3/H_2SO_4/H_2O$ system. T_m denotes the melting point, T_g is the glass point, and T_{crit} is the temperature at which the crystal growth rate overcomes a critical value, ω_{crit}.

this is not necessary for the $HNO_3/H_2SO_4/H_2O$ system under stratospheric conditions because ω_{cryst} is much larger than ω_{nuc}, thus revealing the very small tendency of this system to nucleate and at the same time its ability to rapidly crystallize upon nucleation. This enables the nucleation rate to be determined from bulk freezing experiments. In the limit $\omega_{cryst} \gg \omega_{nuc}$, the statistically averaged freezing rate becomes the nucleation rate and eq 22 reduces to $\omega_{nuc} = \omega_{obs}$. In this case the determined nucleation rates are directly applicable to stratospheric aerosols.

Figure 2 is a schematic plot of the temperature dependence of ω_{nuc} and ω_{cryst} for a solution of given composition and volume in the investigated binary and ternary $HNO_3/H_2SO_4/H_2O$ system. The crystal growth rate is correlated with the supercooling of the liquid, because it is limited by the diffusion of the released latent heat and therefore increases with decreasing temperature below the melting point T_m. At lower temperatures the viscosity of the solution and the diffusion activation energy for the ions in solution become so large that ω_{cryst} decreases again. Unlike ω_{cryst}, the nucleation rate ω_{nuc} needs considerable supercooling before appreciable rates are reached. Due to its highly nonlinear dependence ω_{nuc} then increases steeply and decreases similar to ω_{cryst} when the solution becomes more viscous. Below the glass point, T_g, the viscosity has reached such high values that both ω_{nuc} and ω_{cryst} become negligible, because the liquid has turned into a glass. It remains in this amorphous state irrespective of whether stable germs have been formed during the cooling phase or not. If stable germs are present, crystallization occurs on reasonable time scales only after the sample is warmed up to a temperature, T_{crit}, at which the crystal growth rate overcomes a detectable value, ω_{crit}.

We can define three subregions along the T -axis between T_m and T_g (marked as 1−3 in Figure 2). In region 2, both ω_{nuc} and ω_{cryst} are above the threshold value ω_{crit}, implying nucleation is favorable and crystal growth is sufficiently fast. In region 1, ω_{cryst} is large enough, but ω_{nuc} is too small to induce freezing. In region 3, ω_{nuc} is large enough to lead to the formation of stable germs, which, however, cannot grow because ω_{cryst} is too small. Thus, the liquid state can be maintained for long times, and the liquid crystallizes only upon warming to

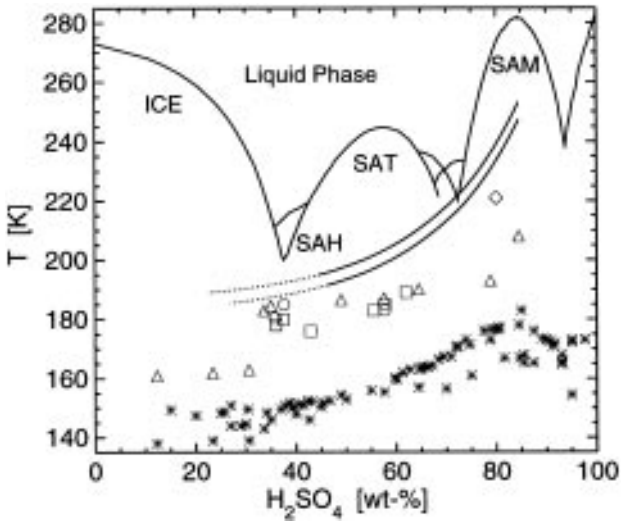

Figure 3. Phase diagram of the binary H_2SO_4/H_2O system[50] together with the glass points T_g and the critical temperatures for fast crystallization T_{crit}. Solid lines are two water uptake curves under stratospherically relevant conditions (for 5 ppmv H_2O at 50 and 100 mbar altitude); the dotted lines are their extensions to lower temperatures and are only relevant under volcanically strongly perturbed conditions. Asterisks are the glass points measured by Vuillard[64] and Ji.[65] Squares, T_{crit} determined by Beyer[30] (heating rate ≈ 2 K/min); triangles, T_{crit} measured by Ji[65] (heating rate 10 K/min); circles, T_{crit} as measured by Zhang[66] (heating rate 4 K/min); diamonds: T_{crit} determined in this work (heating rate 2 K/min).

temperatures around T_{crit}. An important question is to which region liquid aerosols under polar stratospheric conditions belong. As we will show in the following sections, the available laboratory measurements suggest that stratospheric aerosols usually belong to region 1 and sometimes to region 2, while region 3 seems to be achieved only at temperatures well below stratospheric conditions. This reveals that in all cases investigated in laboratory work so far ω_{cryst} is sufficiently large such that ω_{nuc} constitutes the rate-limiting step for freezing.

V. Crystalline versus Amorphous State. It has been proposed by Tabazadeh *et al.*[22] that amorphous glassy aerosols can exist under stratospheric conditions and that these particles do not crystallize despite already being nucleated at low temperatures. This implies that these aerosols would belong in region 3 in Figure 2, and crystallize only upon warming after $\omega_{cryst} > \omega_{crit}$ is reached. Field observations (ER-2 data[20,22] and balloon-borne measurements[40]) seem to support this idea. Alternatively, there is also the possibility that the liquid could convert into an amorphous but nonglassy solid state (called glacial phase) at some low temperature above the glass point (polyamorphism). This has recently been proposed for triphenylphosphite (TPP) by Ha *et al.*[41] However, we show that it is unlikely that such amorphous states exist under stratospheric conditions. Rather, we will show that crystal growth at stratospheric temperatures is fast enough to lead to rapid crystallization of a droplet after nucleation.

It is well-known that H_2SO_4/H_2O solutions readily supercool and form glasses at very low temperatures. The glass points,[42] T_g, have been measured calorimetrically by several authors and are shown in the phase diagram of H_2SO_4/H_2O in Figure 3 (asterisks). Superimposed on the phase diagram are two curves indicating the concentration of a sulfuric acid droplet for typical water partial pressures (5 ppmv H_2O at 50 and 100 mbar total pressure). Clearly, the glass points are about 30 K below the droplet concentration curves, showing that glasses do not exist in the stratosphere. However, this does not yet exclude the

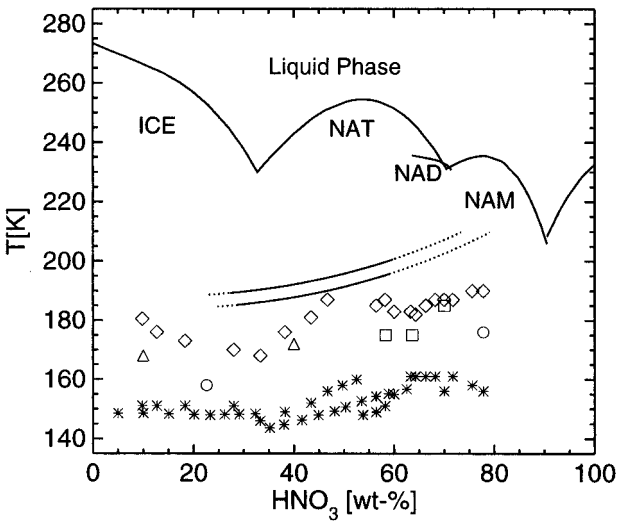

Figure 4. Phase diagram of the binary HNO_3/H_2O system[67] together with glass points T_g and the critical temperatures for fast crystallization T_{crit}. The lines indicate the water uptake curves for the binary HNO_3/H_2O system (for 5 ppmv H_2O at 50 and 100 mbar altitude), while only their solid part is of stratospheric relevance. Asterisks are the glass points measured by Satoh and Kanno[68] and Ji.[65] Diamonds, T_{crit} as measured by Ji[65] (heating rate 3 K/min); triangles, T_{crit} measured by Satoh and Kanno[68] (heating rate not given); squares, T_{crit} measured by Barton *et al.*[45] (heating rate not given); circles, T_{crit} measured by Tolbert *et al.*[46] (heating rate not given).

existence of a nonglassy amorphous state, if the crystal growth were too slow under stratospheric conditions (region 3 in Figure 2).

It is reasonable to assume that the crystal growth rate is zero at the glass point. Hence, if a solution is cooled sufficiently rapidly to temperatures below T_g to avoid freezing, it will not crystallize whether or not stable germs were formed. By slow warming of this sample, it is possible to measure the temperature T_{crit} where the crystal growth becomes fast enough to let the sample freeze. As shown in Figure 3, the measured T_{crit} (squares, triangles, circles, and diamonds) for different compositions are always below the liquid composition curves, although the samples have been warmed up as rapidly as 10 K per minute (slower warming would lead to even lower T_{crit}). This implies that a stratospheric aerosol droplet with a much smaller volume than these samples freezes even faster once nucleated at these temperatures.

Similarly, the glacial phase observed by Ha *et al.*[41] and Cohen *et al.*[43] for TPP is unlikely to occur in H_2SO_4/H_2O solutions under stratospheric conditions. They report the glacial state of TPP to form only at temperatures between 213 and 225 K, which is always below $T_{crit} = 227$ K for the TPP system. The same is true for pure water, where amorphous phases form also only below T_{crit} ($\approx$150 K in this case).[44] Therefore an amorphous state of H_2SO_4/H_2O should not exist under stratospheric conditions which are too warm by at least several kelvins.

The same is true for the binary HNO_3/H_2O system. The phase diagram, together with the glass points (asterisks) and T_{crit} -points (open symbols), is shown in Figure 4. Here, the temperatures T_{crit} were not only determined by means of calorimetric bulk phase measurements but also in aerosol freezing experiments[45] and thin film experiments.[46] The two dotted lines are the water uptake curves for binary HNO_3/H_2O aerosols, while the solid part of these lines indicates the region of stratospherically relevant concentrations and temperatures. Again it is obvious that crystal growth under stratospheric conditions is fast enough to lead to a freezing of binary HNO_3/H_2O aerosols once they are nucleated or seeded.

TABLE 1: T_g and T_{crit} Values for Ternary $H_2SO_4/HNO_3/H_2O$ Solutions

H_2SO_4 (wt %)	HNO_3 (wt %)	T_g (K)	T_{crit} (K)	heating rate (K min^{-1})	ref[a]
25.9	21.2	154	163	<2	1
		152	160	<2	1
14.0	33.1	150	156	<2	1
		151	156	<2	1
7.5	39.5	147	157	<2	1
		150	158	<2	1
3.9	41.2	152	156	<2	1
		152	156	<2	1
2.5	36.3	145	165	<2	1
		145	164	<2	1
43.6	3.5	nm[b]	176	ng[c]	2
39.2	6.0	nm	179	ng	2
38.7	8.6	nm	185	ng	2
22.1	25.1	nm	188	ng	2
9.2	33.0	nm	173	ng	2
7.6	39.5	nm	180	ng	2
53.0	2.3	157	182	4	3
53.0	5.0	158	186	4	3
42.4	2.8	151	184	4	3

[a] References: 1, this work, 2, Beyer;[30] 3, Zhang and Molina, unpublished results. [b] nm, not measured. [c] ng, not given.

There are only a few measurements of T_{crit} for ternary solutions of stratospheric relevance, which are listed in Table 1. Concentrations correspond roughly to aerosols at 50 mbar under volcanically unperturbed conditions. Again, T_{crit} values are well below stratospheric temperatures, as one would expect, because the viscosities of the ternary solutions are between those of the corresponding binary H_2SO_4/H_2O and HNO_3/H_2O solutions.

In addition, all solutions in our experiments that were seeded (with NAT or ice) showed a significant freezing signal within a few minutes, even for temperatures as low as 185 K, which further supports our conclusion. Also, 3 cm^3 of a 40 wt % H_2SO_4/H_2O solution was cooled to a temperature of 186 K and then slowly warmed up to a temperature of 220 K within 6 h without observing a calorimetric freezing or melting signature, suggesting again that ω_{nuc} was too small to induce nucleation at any time. As discussed above, a glacial phase proposed by Ha *et al.*[41] is unlikely to be present in binary or ternary $HNO_3/H_2SO_4/H_2O$ solutions, because it formed only below T_{crit} in their experiments.

As will be shown in section 3, ternary $HNO_3/H_2SO_4/H_2O$ bulk solutions can be supercooled for many minutes to several hours but freeze very rapidly upon seeding. Hence, ω_{nuc} is much smaller than ω_{cryst}, and eq 22 reduces to

$$\omega_{nuc} = \frac{n_{nuc}}{\sum_i t_{obs,i}} = \omega_{obs} \tag{23}$$

allowing upper bounds for nucleation rate coefficients to be determined directly from bulk experiments. These rate coefficients can be applied to stratospheric aerosol droplets to yield upper bounds for homogeneous nucleation as well as estimates for heterogeneous nucleation.

3. Experimental Section

I. Apparatus. The setup used in our freezing experiments is a simple calorimetric device (Figure 5). The sample is contained in a sealable glass tube with an inner diameter of 9 mm and a wall thickness of approximately 1.5 mm. The glass tube is positioned in the liquid ethanol cooling bath of a cryostat with a lowest adjustable temperature of about 183 K. To achieve slow cooling or warming rates and to insulate the sample

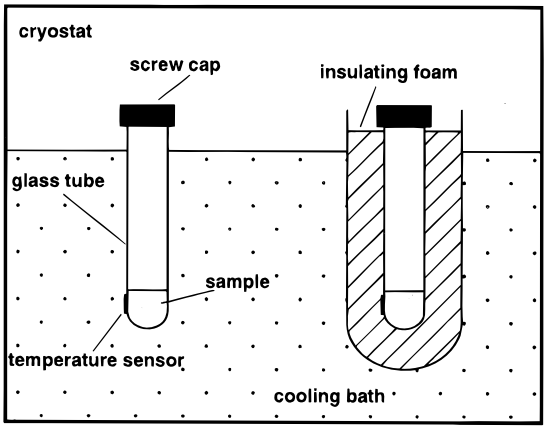

Figure 5. Experimental setup.

from the cooling bath, the glass tube can be positioned alternatively in a second glass with an insulating foam approximately 1 cm in thickness. This is especially useful for the detection of the melting and eutectic points during warming, because the temperature is very stable inside the insulation, which facilitates the detection of gradual changes of latent heat. The two low-mass (3.5 mg) sensors for simultaneous temperature measurements have a resistance of about 70 Ω at room temperature and are connected to a parallel circuit and an autoranging picoampere meter. The electric current flowing through the sensors and the circuit board is approximately 10 μA and stable within 0.05%. The ampere meters are connected to a PC via an IEEE card, and the evaluation software collects 1 data point every 2 s. The sensors are calibrated in the temperature range between 177.80 K (melting point of acetone) and 273.15 K (melting point of water ice) and for the determination of the glass points down to the boiling point of liquid nitrogen (77.35 K). The relative temperature accuracy of the sensor and the electronics is better than ±0.1 K, while the absolute accuracy is ±0.7 K for $T > 175$ K and approximately ±2 K for $T < 175$ K.

With a minimum measuring time of 100 s (limited by the crystal growth time) and an upper practical time limit of 10 h, the range of homogeneous nucleation rates that can be determined is limited by the experimental sample volumes, which were typically 0.5−4 cm^3. Thus, the minimum homogeneous nucleation rate J_{min} is given by $J_{min} = 1/(4\ cm^3 \times 10\ h) \simeq 10^{-5}\ cm^{-3}\ s^{-1}$, and the maximum homogeneous rate $J_{max} = 1/(0.5\ cm^3 \times 100\ s) \simeq 10^{-2}\ cm^{-3}\ s^{-1}$. If the nucleation rate of the investigated system is larger than J_{max}, no further information about its value can be deduced. However, if it is smaller than J_{min} an upper rate can be estimated from eq 11.

II. Advantages and Disadvantages of Bulk Experiments. Nucleation studies cannot normally be performed using bulk experiments because the presence of dust particles and the containment walls induce heterogeneous nucleation. For many systems fast heterogeneous nucleation means that bulk freezing temperatures are not far below the melting temperature, whereas small aerosol particles of the same composition freeze at much lower temperatures due to homogeneous nucleation.[47] Not much can be learned from bulk experiments under these conditions. On the other hand, if the nature of the investigated system is such that the supersaturations and temperatures of interest can be reached in a bulk experiment without nucleation, aerosol particles will not freeze either when subject to the same conditions. Under these circumstances a bulk experiment is actually the better experiment, because it allows a much lower value for an upper bound of the homogeneous nucleation rate to be determined. For stratospheric aerosols the upper bounds given in the present paper are sufficient to exclude the possibility of homogeneous freezing of the aerosol with equilibrium conditions above the frost point, thus corroborating our earlier results.[21]

It could be argued that in a bulk experiment a solution would be exposed to uncontrolled HNO_3 and H_2O partial pressures and that this could influence nucleation at the gas/liquid interface. However, this is not true as the solution readily establishes the correct thermodynamic vapor pressures in the small gaseous volume above its surface. Only the total pressure is different, but a dependence of phase transitions on the carrier gas pressure is not expected nor has it been observed in experiments to $p < 10$ mbar.[48] Since the vapor pressures above the solution are usually not measured in a bulk experiment, the chosen combination of HNO_3, H_2SO_4, and H_2O concentrations and temperature does of course rely on thermodynamic models for the liquid phase.[1,2,49] These models have now become widely accepted, and with our experiment we can probe a range of conditions around those predicted by the models. With this caveat in mind, thermodynamic equilibrium between bulk and gas can always be reached unless the applied cooling rates are too high. In this case sublimative nucleation of the hydrates on the containment walls is provoked, which leads to seeding of the solution and therefore to artificially enhanced nucleation rates (see next subsection).

Another argument against bulk experiments could be that they are not suited for obtaining information on the formation of metastable hydrates (like $HNO_3 \cdot nH_2O$, $n = 2, 5, 10, ...$,[17,18] $H_2SO_4 \cdot nH_2O$, $n = 2, 3, 6.5, 8, ...$,[50,51] and mixed H_2SO_4/HNO_3 hydrates[19]). It is indeed true that the isolation of metastables under highly supersaturated conditions with respect to a stable phase is difficult, if not impossible, in bulk solutions, because stable phases readily assume control. In contrast, isolation of metastables has been achieved in single-particle experiments.[47] However, there is no reason why metastables cannot crystallize in bulk solutions, and indeed we did observe NAD and SAH in our experiments (see, for example, Figure 1). Formation of a metastable crystal is a first-order phase transition accompanied by the release of latent heat that can be measured. On the other hand, in our experiments usually no phase transitions were observed at all; hence, the nucleation of both stable and metastable crystals can be excluded.

In essence, the main advantage of bulk freezing experiments becomes evident in the case that no nucleation occurs, which leads to a smaller and therefore better confined upper bound for the homogeneous rate coefficient of stable and metastable crystals than with aerosol experiments. When rapid nucleation takes place in the bulk, the freezing of aerosols under the same conditions is possible but by far not proven. Then aerosol experiments have to be applied.

III. Rate Measurements. In this section we apply the statistics described in section 2 to bulk freezing experiments. We will show that nucleation indeed behaves according to Poisson statistics. Figure 6 shows results for an HNO_3/H_2O solution with a concentration of 53.8 wt % (i.e. a 1:3 stoichiometry corresponding to nitric acid trihydrate, NAT) and a volume of 3 cm^3 at a temperature of 226 K. The probability to observe no freezing, $P_0(t)$, is plotted as a function of time with the individual points calculated as $n_{liq}(t)/n_{tot}$ following eq 5. Despite the small number of data points, the exponential behavior is clearly revealed as expected for a stochastic process. Note that the solid line is not a least-squares fit to the data, but the rate calculated from Poisson statistics using eq 9. The rate ω is calculated to be $4.1 \times 10^{-3}\ s^{-1}$, which yields a homogeneous nucleation rate coefficient $J = 1.4 \times 10^{-3}\ cm^{-3}$

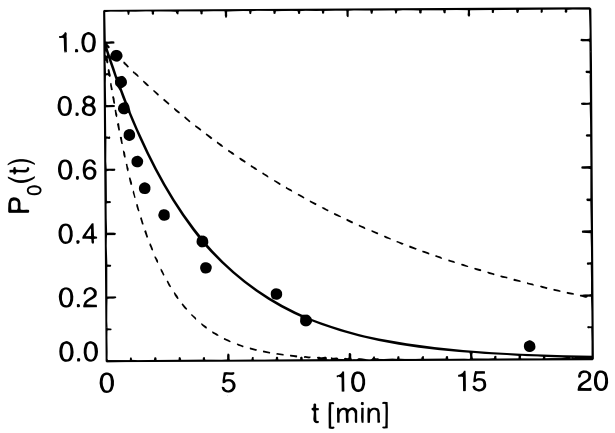

Figure 6. Probability to remain liquid, $P_0(t)$, versus time for 53.8 wt % HNO_3/H_2O solutions (i.e. a 1:3 stoichiometry) at 226 K. The sample volume was 3 cm^3. The line is the corresponding exponential curve with the rate coefficient calculated by Poisson statistics; the dashed lines indicate the upper and lower fiducial limits for the rate coefficient on a confidence level of 0.999.

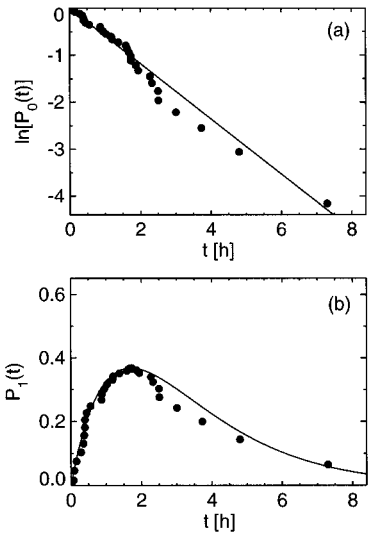

Figure 7. (a) Probability to remain liquid, $P_0(t)$, versus time for 3 cm^3 solutions with 21.5 wt % H_2SO_4 and 20.0 wt % HNO_3 at 188.3 K. Data points from Beyer,[30] solid curve determined from Poisson statistics (eq 5). (b) Probability of observing exactly one freezing event, $P_1(t)$, versus time for the same data set. The line is calculated from eq 6.

s^{-1} assuming homogeneous nucleation to be the fastest individual nucleation process. The upper and lower statistical fiducial limits for J on a confidence level of 0.999 are 3.1×10^{-3} cm^{-3} s^{-1} and 4.6×10^{-4} cm^{-3} s^{-1}, respectively, as calculated from eqs 10a,b and are also shown in Figure 6 (dashed lines). Clearly, the true homogeneous nucleation rate is smaller than the upper fiducial limit with a probability of 0.999. It could even be smaller than the lower fiducial limit when the freezing is due to heterogeneous nucleation.

Figure 7a shows $P_0(t)$ for a ternary solution (21.5 wt % H_2SO_4, 20.0 wt % HNO_3, volume 3 cm^3) at 188.3 K measured by Beyer.[30] These data are in good agreement with the theoretical prediction of an exponential decay over many orders of magnitude (solid line determined from Poisson statistics). For the same solution, Figure 7b shows the probability to observe exactly one freezing event, $P_1(t)$, as a function of t as calculated from eq 6. Again the experiment can be described by Poisson statistics. Exponential decay was also observed in smaller bulk samples[37] and in aerosol experiments with supercooled H_2O droplets[52] or binary HNO_3/H_2O droplets[34] clearly

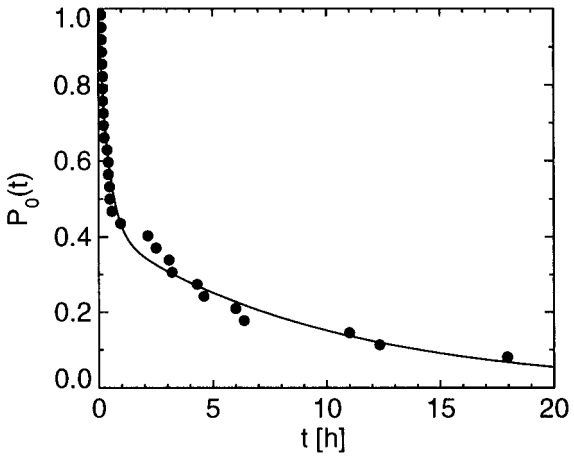

Figure 8. Probability to remain liquid, $P_0(t)$, versus time for 0.03 cm^3 solutions with 9.1 wt % H_2SO_4 and 33.1 wt % HNO_3 at 193 K[30] together with the line calculated by eq 19. The two different processes are clearly visible.

showing that the Poisson statistics derived here describes the nucleation process independently of sample volume.

As outlined in section 2.III, freezing experiments do not always behave as a statistically homogeneous ensemble revealing a single-exponential decay law. In Figure 8 we show a typical example of a statistically inhomogeneous ensemble. These are measurements of a ternary solution (9.1 wt % H_2SO_4, 33.1 wt % HNO_3, volume 0.03 cm^3) at 193 K measured by Beyer.[30] Two different subsets of the ensemble are clearly distinguishable. The solid line is a fit to the data on the basis of eq 19. A subset of 18 of the 31 samples ($\alpha = 0.581$) is subject to a fast process with a rate ω_{fast}, while the other 13 show a much smaller rate ω_{slow}. The two rates differ by more than 1 order of magnitude. We find $\omega_{fast} = 6.8 \times 10^{-4}$ s^{-1} and $\omega_{slow} = 2.8 \times 10^{-5}$ s^{-1} corresponding to $J_{slow} = 9.4 \times 10^{-4}$ cm^{-3} s^{-1}. Without this separation, the overall rate as calculated from eq 9 would give $\omega_{tot} = 6.3 \times 10^{-5}$ s^{-1} resulting in $J_{tot} = 2.1 \times 10^{-3}$ cm^{-3} s^{-1}. Thus, the neglect of an experimentally-induced fast heterogeneous process within a subset of the samples leads to an overestimation of the nucleation rate by more than a factor of 2. Similar examples showing distinct subsets can be found in the measurements of Beyer.[30]

Figure 9a shows a similar case of heterogeneously-enhanced freezing in a subset of H_2SO_4/H_2O solution samples (51.8 wt %) taken from Beyer.[30] Out of a total of 16 samples, 10 nucleated with freezing times shorter than 6.4 h (solid circles) while the other 6 remained liquid within the observation time of 24 h (open circles). The dotted line represents a fit to all data using Poisson statistics and assuming a single common freezing mechanism, which obviously does not lead to an adequate description of the experiment. This suggests that there are at least two different processes involved, one slow enough to allow some samples to remain liquid for 1 day, and one rapid enough to make the remaining samples freeze within 6 h. We calculate the upper fiducial limit for the samples which did not freeze and the lower fiducial limit for the ones which did (eqs 10a and 11) and find that they belong to different processes with a probability of 99.9987%. Using only the frozen samples, we recalculate the rate according to Poisson statistics and find that the data points and the exponential law are in excellent agreement (Figure 9b), revealing that heterogeneous nucleation is also a stochastic process. The upper limit for ω for the samples which did not freeze is 1.3×10^{-5} s^{-1} on a confidence level of 0.999, giving an upper limit of 4.3×10^{-6} cm^{-3} s^{-1} for homogeneous nucleation under these conditions.

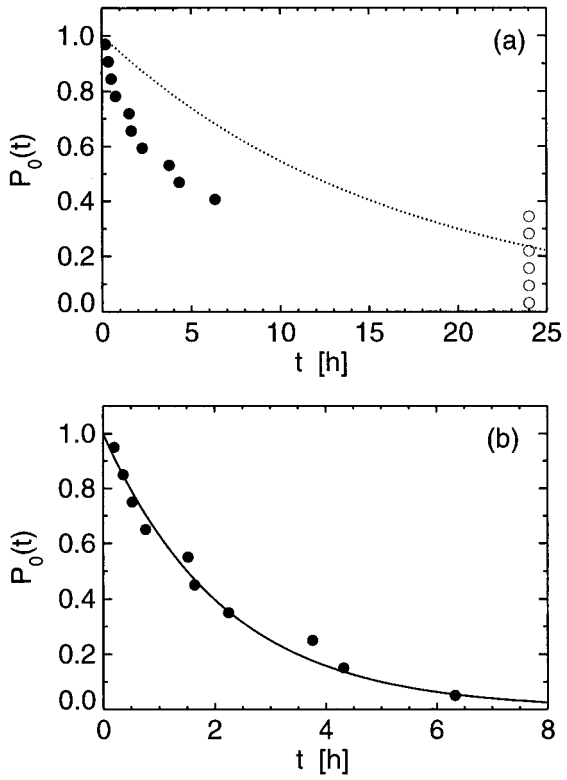

Figure 9. (a) Probability to remain liquid, $P_0(t)$, versus time for 3 cm^3 binary H_2SO_4/H_2O solutions with 51.8 wt % as measured by Beyer.[30] Solid circles, freezing times of different samples; open circles, samples which did not freeze within the observation time of 24 h; dotted line, exponential curve as calculated by Poisson statistics taking into account all data points. (b) Same data as in (a) without the unfrozen samples; solid line, exponential curve as calculated by Poisson statistics taking into account only the frozen sample data points.

One important reason for the appearance of two independent and very different rates is closely related to the experimental cooling process of a solution during the transfer from room temperature to stratospheric conditions. As we have shown in our previous work[21] in most of the investigated binary and ternary solutions, freezing can be avoided if the cooling of the samples is performed very slowly. During cooling, substantial amounts of vapor have to condense onto the liquid or the glass walls in order to reduce the partial pressures from typically 10 mbar of H_2O and 0.1 mbar of HNO_3 to the approximately 4 orders of magnitude lower stratospheric values. With very low cooling rates, these gas phase molecules are taken up by the liquid and nucleation of liquid or solid condensates on the glass walls is avoided. On the other hand, when the cooling was very rapid in our experiments, condensates often became visible on the glass walls. Rapid cooling may yield vapor supersaturations of 10^4 and higher, which inevitably leads to the nucleation of liquid and solid condensates on all available surfaces. If the bulk solution comes into contact with the condensation products, these may act as seeds and trigger the freezing of the entire sample. The seeding may be forced by gently tipping the glass tube to establish contact with the condensates in the vicinity of the meniscus of the liquid. The unintended seeding effect is aggravated if, during rapid cooling, the containment walls become much colder than the solution because of their direct contact with the cooling agent. This seeding mechanism is an experimental artifact, which does not necessarily show an exponential behavior. This mechanism is also the most likely explanation for the observations by Barlow and Haymet[37] that about one-third of their water samples froze rapidly during the cooling process while the remaining samples, once they reached the final temperature, showed a slower freezing rate.

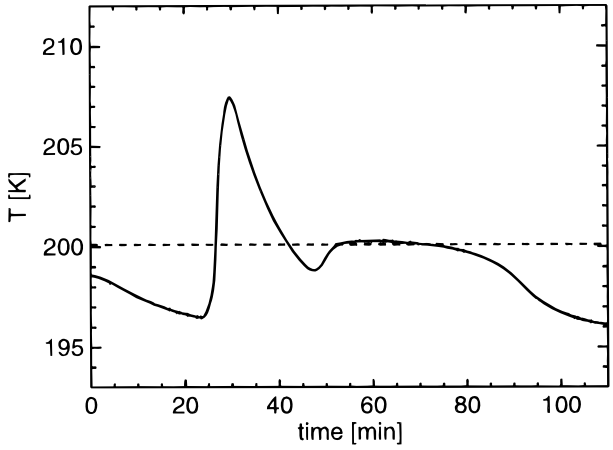

Figure 10. Freezing experiment of a 50 wt % H_2SO_4/H_2O binary solution showing the temperature evolution of the sample. The first peak corresponds to the crystallizing to SAT, the second to the eutectic growth of SAT and ice after ice has nucleated. The dashed line gives the temperature of the SAT/ice eutectic.

There are also cases in which a separation into two rates can be explained by other microphysical processes, for example, when a sample subset offers additional heterogeneous surfaces like dust particles or differences in the glass wall of the tubes (scratches etc). In this context it is important to note that bulk experiments do not always reveal an exponential decay: The stochastic behavior may be absent due to seeding after rapid cooling or because of the irreproducibility of the surface morphology in different containment vessels and its influence on heterogeneous nucleation. Numerous examples of this type can be found in Beyer.[30]

IV. Freezing Behavior of the Binary H_2SO_4/H_2O System. A typical example of the temperature signal for a freezing experiment with a binary H_2SO_4/H_2O solution (50 wt %) is shown in Figure 10. From the solution, SAT nucleates at 196.5 K leading to a steep rise in temperature due to the release of latent heat with a maximum at approximately 207 K. Upon crystallization of SAT, the solution becomes more dilute and the ice saturation ratio increases. When the temperature has again fallen to about 1.5 K below the SAT/ice eutectic temperature[50] (≈200 K), ice nucleates and the sample warms up to the eutectic temperature as SAT and ice crystallize as a eutectic mixture. In a subsequent warming cycle (not shown), the measured melting points of the sample agree well with the binary phase diagram of Gable *et al.*,[50] showing that indeed SAT and ice were the freezing products.

We have performed freezing experiments covering the entire concentration range of stratospheric interest between 40 and 84.5 wt %. As a general pattern the experiments demonstrate that none of the solutions froze readily and that in case of nucleation, SAT was the most common freezing product in the range between 40 and 57.6 wt %. While SAT is to be expected for concentrations near the 1:4 stoichiometry (57.6 wt %), it is quite surprising that SAT freezes from a 1:6.5 solution (45.6 wt %). In the 1:6.5 solution for higher temperatures, SAT was the usual freezing product, while below ≈189 K sometimes SAT and sometimes SAH crystallized. Interestingly, SAT froze more readily from more dilute solutions than from the one with the ideal stoichiometry of 1:4, the maximum in freezing rates appearing to be in the region around 48−50 wt %. This maximum was also observed by Beyer *et al.*;[31] however, they did not analyze their freezing products. As we have argued above, freezing in these cases is most likely due to heteroge-

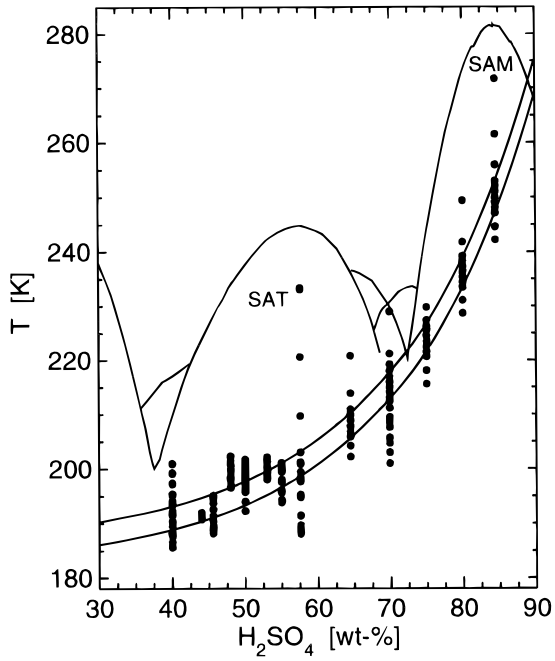

Figure 11. Overview of experimentally determined upper bounds for homogeneous nucleation rates superimposed on the H_2SO_4/H_2O binary phase diagram. Data points, concentrations and temperatures with a measured homogeneous nucleation rate lower than 1×10^{-2} cm^{-3} s^{-1} on a confidence level of 0.999; solid lines, water uptake curves showing the stratospheric aerosol concentration for 5 ppmv H_2O at 50 and 100 mbar altitudes.

neous nucleation on the glass walls or dust particles (at the same time the formation of ice was carefully avoided), and this might indicate that SAT is more compatible with the available surfaces than SAH, while both compatibilities are poor. Also, it cannot be excluded that SAH nucleated first even in the cases where SAT was the final product.

An overview of the obtained upper bounds for homogeneous nucleation rates is given in Figure 11. Each point corresponds to a homogeneous nucleation rate of at most 1×10^{-2} cm^{-3} s^{-1} at the indicated concentration and temperature on a confidence level of 0.999. The two lines are the water uptake curves for a mixing ratio of 5 ppmv at H_2O typical stratospheric altitudes of 50 and 100 mbar, describing the concentration of H_2SO_4 aerosol droplets as a function of temperature under these conditions. As can be seen, neither SAT nor sulfuric acid monohydrate (SAM, $H_2SO_4 \cdot H_2O$), the two most prominent crystalline phases, nucleate readily. All the examined solutions exhibited very small nucleation rates revealing that homogeneous freezing of stratospheric binary H_2SO_4/H_2O aerosols is an unimportant mechanism.

Significantly higher freezing temperatures for solutions between 44 and 60 wt % have been reported by Ohtake.[29] He cooled solutions rapidly (within 1 or 2 min) from room temperature to the desired temperature of 190−200 K by suspending the warm sample directly into the cold bath. Under similar conditions we observed the formation of small ice crystals on the walls which can trigger heterogeneous freezing when brought into contact with the solution in the vicinity of the meniscus, as outlined above. Already Ohtake[29] mentioned that frost on the tube walls tended to seed the solutions. We believe that this process is the reason for the much higher freezing points than with slow cooling. Clearly, the lower the measured freezing rate, the better determined the upper bound for homogeneous nucleation. To avoid the formation of ice frost, we cooled the solutions very slowly to achieve a small temperature gradient within the sample. Then the formation

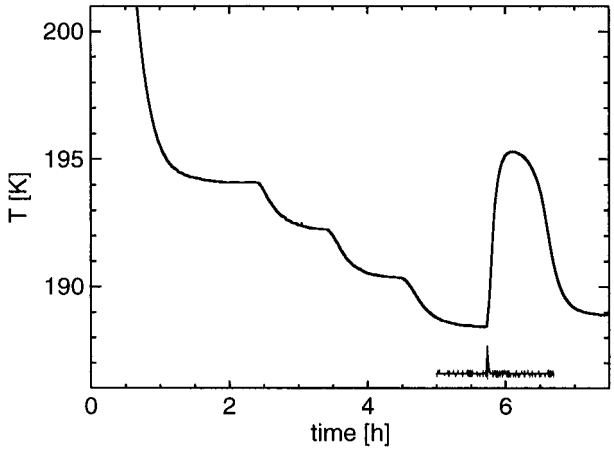

Figure 12. Freezing experiment of a 40 wt % H_2SO_4/H_2O binary solution showing the temperature evolution of the sample. The small peak on the line in the lower right indicates the time when the sample was seeded with a small ice pellet.

of ice is not favorable at any time, because the vapor pressure of ice is higher than that of the solution at the same temperature. We tested this with different solutions and indeed found that we could go to much lower temperatures without freezing of the samples.

Conversely, the crystallization of H_2SO_4/H_2O solutions can be forced by seeding with ice pellets. To show that heterogeneous nucleation of H_2SO_4 hydrates on ice might be of stratospheric relevance, a record of an experiment with a solution of 40 wt % is plotted in Figure 12. This solution could be supercooled stepwise for hours without freezing, before it was seeded with a small ice pellet at 188.5 K. At this point, concentration and temperature are very similar to a binary aerosol droplet at the frost point under strongly denitrified Antarctic conditions (see Figure 3). The instantaneous rise in temperature is most likely due to the nucleation of SAT and freezing of the whole sample. Though at first sight surprising, the steepness of the temperature rise of the sample at such a low temperature and unfavorable concentration can be explained by the eutectic growth of ice and SAT. Eutectic growth is often found to be much faster than that of the single components under the same conditions: Liquid phase diffusion no longer limits the growth, because molecules have to diffuse only over small distances. Another possible explanation for the steep rise in temperature could be that seeding with ice initiates the nucleation of sulfuric acid octahydrate (SAO, $H_2SO_4 \cdot 8H_2O$), since the solution has almost the required stoichiometry (1:8.2). The melting of this sample (not shown) does not allow a clear distinction to be made between SAT and SAO: Two plateaus at 200 and 207 K could be either due to the eutectic melting of SAT and ice followed by the melting of the remaining SAT or due to the peritectic transformation of SAO to SAT and liquid (which is also endothermic) followed by the melting of SAT. However, a comparison with the thin film experiments of Middlebrook *et al.*[53] suggests the formation of SAT instead of SAO. In their experiments liquid H_2SO_4/H_2O films froze when the samples were cooled 1−4 K below the ice frost point. The freezing products were always ice and SAT, suggesting that ice was freezing from the solution below the frost point forcing SAT to nucleate heterogeneously on the ice surface, which agrees with the above interpretation that ice facilitates the nucleation of SAT. However, because the ice surface in both experiments was large compared to ice crystals in stratospheric aerosols, we do not know whether heterogeneous nucleation is fast enough to lead to freezing of SAT below the frost point in

the stratosphere. The answer to this can only come from aerosol experiments.

We also conducted seeding experiments to investigate the ability of several other agents to enhance freezing of a solution with a stoichiometry of 1:4 (57.6 wt %) via heterogeneous nucleation by suspending different substrates of stratospheric relevance with macroscopic surface areas of at least 10^{-2} cm^2. The investigated agents, Al_2O_3 (representative of exhaust of solid-propellant rocket motors), Fe_2O_3 and Fe_3O_4 (major constituents of meteoritic dust particles), $(NH_4)_2SO_4$ (possible minor constituent of stratospheric aerosol particles), and AgI (known as a good ice nucleus), did not significantly enhance the freezing probability. We estimate the upper bound for the heterogeneous nucleation rate on any of these agents to be 1 cm^{-2} s^{-1} on a confidence level of $x = 0.999$. For original micrometeorites or other meteoritic material, we have shown that there is a possible enhancement of the freezing rate, but this does not suffice to explain freezing of stratospheric clouds ($j \leq 4$ cm^{-2} s^{-1}).[54] Also pure and oxidized graphite laminate and activated carbon were tested as a proxy for soot from aircraft exhaust but did not show enhanced freezing.[55]

In addition, it should be noted that our solutions were not filtered but exposed to laboratory air during preparation, so they probably contain many undissolved particles of tropospheric origin in the 1−10 μm range. In essence, not only homogeneous but even heterogeneous nucleation of stratospheric binary H_2SO_4/H_2O aerosol droplets appears to be an unlikely freezing mechanism unless the stratosphere provides other nuclei much better suited for heterogeneous nucleation than were present in our experiments.

In the following, the H_2SO_4/H_2O freezing experiments are compared with the results of classical nucleation theory for the freezing of SAT as presented by Luo *et al.*[56] These authors compared the theoretical results for heterogeneous nucleation (their Figure 3a) with measurements performed by Ohtake.[29] The present investigation offers a much better constrained analysis of nucleation theory.

We have used the experimentally determined maximum rates for homogeneous nucleation (see Figure 11) as an upper bound for the theoretical calculations and, with the arguments given in sections 2.IV and 2.V, the glass points as a lower bound (see Figure 3). Cooling a concentrated H_2SO_4/H_2O solution to below its glass points usually led to the sample freezing upon warming, suggesting that there is a region of sufficiently high nucleation rates between these two bounds.

Our present work differs from the original analysis done by Luo *et al.* in two important ways. First, the present work suggests that homogeneous and heterogeneous nucleation rates are considerably below the upper limits given by Ohtake's rapid cooling experiments. This shifts the region of maximum freezing probability around 50 wt % to lower temperatures, and hence, the theoretical treatment given by Luo *et al.* will not be able to reproduce the new measurements. However, agreement with the new experiments can be established if the diffusion activation energy of the sulfate ions in solution is lower than estimated by Luo *et al.*, while at the same time the Gibbs free energy is larger. This shifts the region of maximum nucleation probabilities to lower temperatures.

Second, as mentioned above the probability that the bulk solutions (1 cm^3) freeze as SAT does not reach its maximum at 1:4 stoichiometry, but rather at lower concentrations (about 48−50 wt %).

Luo *et al.*[56] estimated diffusion activation energies for the H_2SO_4/H_2O solutions Δg_{sol} from viscosities of these solutions. Since viscosities increase considerably with concentration at a fixed temperature, this introduces in principle the observed asymmetry in the nucleation data. Luo *et al.* then derive the diffusion activation energy of the acidic ions, Δg_a, from Δg_{sol} by estimating the difference in the bonding energy of the acidic ions as compared to water molecules and found Δg_a to be substantially larger than Δg_{sol}. The enhancement factor depends on the partial heat of vaporization of H_2SO_4 from the solution, which is larger for more dilute solutions, hence opposing the observed asymmetry.

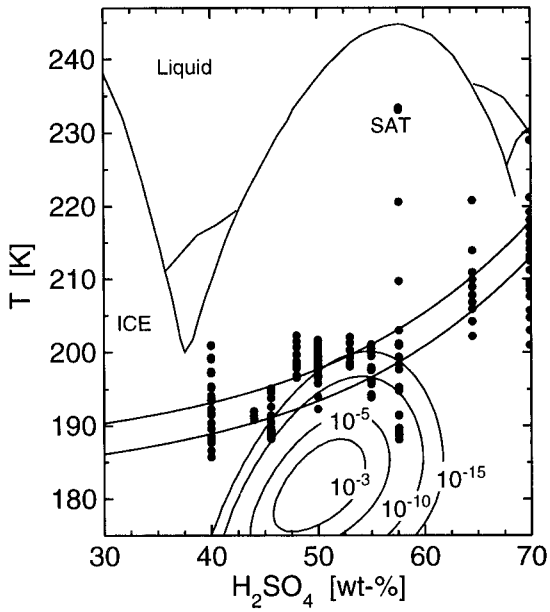

Figure 13. Comparison of model calculated homogeneous nucleation rates (contours; in cm^{-3} s^{-1}) and experimentally determined upper bounds (solid points correspond to a rate $J \leq 10^{-2}$ cm^{-3} s^{-1}).

In contrast to this treatment, the present data suggest that the diffusion activation energy of the acid ions is not very different from that of the solution. In the following we repeat the calculations of Luo *et al.* with the following changes: (i) we use $\Delta g_a = 1.1 \Delta g_{sol}$; (ii) we fit Δg_{sol} from the viscosity data by Schäfer[57] and Williams and Golden[58] and in addition to the more recent data by Williams and Long;[59] (iii) we increase the solid/liquid interface energy by a factor of 1.35 over the function $\sigma_{sl}(c, T)$ used by Luo *et al.* (deviations of this magnitude had been discussed by these authors).

We can now re-examine the behavior of homogeneous nucleation using the present parametrization. Figure 13 shows the H_2SO_4/H_2O phase diagram including the updated version of the homogeneous nucleation rates. The figure is directly comparable with Figure 3b of Luo *et al.* The maximum nucleation probability now lies at lower temperatures and concentrations. However, the main conclusion reached by Luo *et al.* that homogeneous nucleation would not lead to any substantial freezing of the stratospheric aerosol is fully corroborated.

The new parametrization can also be used to investigate heterogeneous nucleation rates of SAT and the compatibility of SAT with different substrates. We show this as an example for a 50 wt % H_2SO_4/H_2O solution at 195 K. The experimentally determined upper bound for the rate coefficient for heterogeneous nucleation of SAT on the glass walls (with a surface area $A \simeq 10$ cm^2) is 10^{-2} cm^{-2} s^{-1}, revealing a maximum compatibility for SAT on glass of $m = 0.02$ under these conditions as calculated with the help of nucleation theory. On the other hand, we can estimate how likely heterogeneous nucleation could lead to freezing of a stratospheric aerosol droplet. Under the same conditions and assuming one nucleus

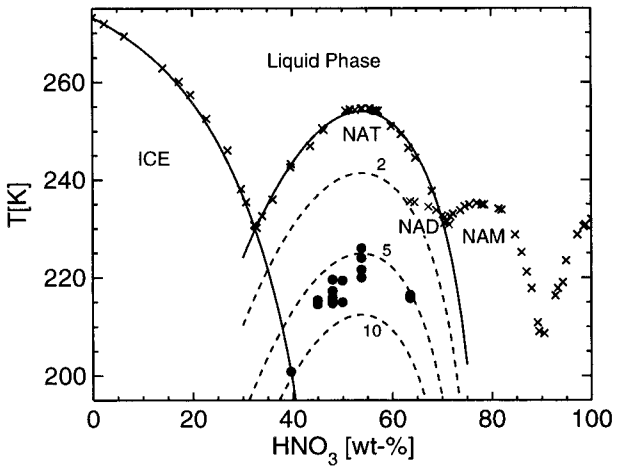

Figure 14. Freezing temperatures of binary HNO_3/H_2O solutions 1 cm^3 in volume. The crosses indicate the melting points measured by Küster and Kremann[67] and Ji.[65] The solid lines give the melting points of ice and NAT as calculated with our model. The dashed lines give the temperatures and concentrations at which the saturation ratio of the liquid with respect to NAT is 2, 5, and 10.

with a surface area of $A \simeq 10^{-11}$ cm^2 ($r \simeq 10$ nm) in a droplet, a stratospherically relevant nucleation rate corresponding to a characteristic freezing time of about 1 month would require a much higher compatibility of at least 0.37. Substrates of these compatibilities have not been found yet, and the existence of such nuclei in the stratosphere seems to be unlikely in view of the many heterogeneous samples tested in our work.[21,54,55]

V. Freezing Behavior of the Binary HNO_3/H_2O System. Meilinger *et al.*[23] have shown that liquid stratospheric aerosols can depart considerably from thermodynamic equilibrium compositions caused by rapid temperature fluctuations, for example, in orographically-forced lee waves. Their calculations suggest that HNO_3 uptake by larger droplets is diffusively hindered, while small droplets can approach the composition of binary HNO_3/H_2O solutions with up to 52 wt % of HNO_3. Therefore, we conducted several experiments with HNO_3/H_2O solutions (1 cm^3) in the concentration range of 45−63.6 wt % corresponding to stoichiometric ratios of 1:4.3 to 1:2, respectively.

Figure 14 shows the freezing points of these solutions in the temperature range between 214 and 226 K. The freezing usually occurs at saturation ratios with respect to NAT, S_{NAT}, of between 5 and 10. The samples were cooled rapidly to temperatures of about 225 K and then slowly to lower temperatures. This was to avoid the formation of ice and NAT on the glass walls from the vapor phase, and the glass tubes were checked repeatedly for signs of frost.[60]

We could not supercool binary $HNO_3/H_2SO_4/H_2O$ solutions between 45 and 63.6 wt % to temperatures of stratospheric interest without freezing. This might be due to heterogeneous nucleation from the liquid on the glass wall or on dust particles in the unfiltered samples. Another possible explanation is that even the homogeneous nucleation rates at these temperatures are high enough to induce freezing in our samples. With our setup we are limited to homogeneous nucleation rates smaller than approximately 10^{-2} cm^{-3} s^{-1}, because the bulk samples are at least 1 cm^3 in volume. Hence, the homogeneous nucleation rates in the binary HNO_3/H_2O samples are probably larger than 10^{-2} cm^{-3} s^{-1}; however, we cannot determine the actual value at these or even lower temperatures. As will be discussed below, binary and almost binary HNO_3/H_2O solutions were found to be the only solutions which could not be supercooled to stratospheric temperatures. This might indicate that aerosol droplets with these concentrations could indeed freeze homogeneously under stratospheric conditions. An answer to this question can only come from aerosol experiments, enabling nucleation rates above a certain (high) value to be measured, whereas bulk experiments are needed to measure low nucleation rates. In this way aerosol and bulk experiments complement each other. Disselkamp *et al.*[34] have shown in aerosol chamber experiments that the rate coefficient for homogeneous nucleation of nitric acid dihydrate (NAD) from droplets with a composition of 1:2 (≈63.6 wt %) are of the order of 10^8−10^{10} cm^{-3} s^{-1} in the temperature range of 193−204 K, thus supporting our hypothesis of a possible freezing of binary and almost binary HNO_3/H_2O aerosols at stratospheric temperatures. However, further work is needed to evaluate a broader concentration and temperature range.

VI. Freezing Behavior of the Ternary $HNO_3/H_2SO_4/H_2O$ System. Calorimetric measurements require the knowledge of melting points of the binary and ternary systems to identify the frozen solid phases and to determine the saturation ratio of the liquid with respect to a solid phase. However, melting points of NAT, SAT, etc. over the entire ternary concentration range of stratospheric interest have not been measured so far. Therefore we have calculated the ternary phase diagram using a thermodynamic model (a parametrization of which is given in Luo *et al.*[49]). The semiempirical model is of the Pitzer ion interaction type and is able to predict liquid phase activities for H_2O, H_2SO_4, and HNO_3 in the concentration range wt %(H_2SO_4) + wt %(HNO_3) $\lesssim$ 70 wt % and for temperatures 185 K $\leq T \leq$ 400 K. The activity products of the solid phases are calculated from the model using experimental freezing points (above the eutectics) and vapor pressure measurements over solid phases (below the eutectics). Koop *et al.*[21] have shown that crystallization and melting of ternary samples can be understood with the help of the ternary phase diagram and that the measured melting points are in very good agreement with the ones calculated from the model.

We repeat this analysis here for another interesting case, the melting of hydrates in a solution more concentrated in sulfuric acid than in the case investigated by Koop *et al.*[21] A measurement of the melting points of a ternary solution with 21.2 wt % HNO_3 and 25.9 wt % H_2SO_4, which froze after cooling to 182 K, is shown in Figure 15. In the lower part of the figure we show the calorimetric temperature development during slow heating of the sample. Three plateaus are clearly visible, each belonging to the complete melting of one solid phase. To determine the exact eutectic and melting points we calculated the derivative of the temperature with respect to time (dT/dt) which is shown in the upper part of the figure. The measured plateau temperatures are in good agreement with the phase diagram in Figure 16 calculated from the thermodynamic model. The thin solid and dotted lines represent isothermal cuts through the ternary phase diagram indicating the coexistence curves of NAT, SAT, and ice with the ternary liquid at 194.7, 219.7, and 239.5 K.

Upon warming, the system reaches the measured ternary eutectic point at 193.7 K (Figure 15). The eutectic point is characterized by the intersection of the three coexistence curves (marked as point 1 in Figure 16a), where all three solids coexist with a ternary liquid of 35.4 wt % H_2SO_4 and 1.8 wt % HNO_3. The experimentally determined eutectic temperature (193.7 K) agrees with the model value (194.7 K) to within 1 K. After the ice has completely melted, the system leaves the eutectic point and the temperature rises. The system then slides along the NAT/SAT/liquid coexistence curve, constantly melting NAT and SAT. This defines the thick solid line between points 1

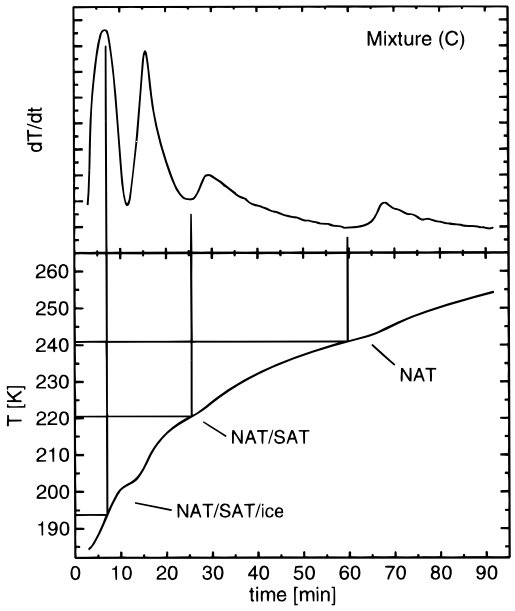

Figure 15. Warming curve of a frozen ternary sample containing 21.2 wt % of HNO_3 and 25.9 wt % of H_2SO_4. The lower section gives the temperature evolution of the sample, while the upper section shows the derivative of the temperature with respect to time. The melting points of the solid phases are extracted in two different ways: First, the eutectic melting point is defined by a fixed temperature, at which the completely frozen sample (NAT/SAT/ice) starts to absorb latent heat. Hence, dT/dt decreases strongly, the onset of which is marked by a maximum in dT/dt. In the ideal case dT/dt should fall to zero instantaneously, but due to the finite heat capacities and temperature gradients in the present cryo-system, a minimum in dT/dt is only reached after a certain time delay. Second, the remaining solid phases (NAT and SAT) melt continuously over a temperature range, and each melting point is defined as the temperature when the respective crystal has completely melted. Because at this point latent heat is no longer absorbed by the sample, this leads again to a rise in the temperature curve, i.e. a minimum in dT/dt.

and 2 in Figure 16b. The second plateau is reached at about 220.5 K, which can be identified as that point on the NAT/SAT/liquid coexistence curve where the remaining SAT melts (point 2 in Figure 16b). Now only NAT is left, which melts at about 240.9 K, where the system leaves the NAT stability region (point 3 in Figure 16c, which corresponds to the overall concentration of the sample). The slope of the thick straight line between points 2 and 3 in Figures 16b,c is constructed from simple stoichiometric considerations.[61] Again, the model-predicted melting points of SAT and NAT at 219.7 and 239.5 K, respectively, agree with the measured values (220.5 and 240.9 K) to within 1.4 K. However, it should be noted that the uncertainties in both experimental and model-predicted melting points are ±2 K.

Finally we turn to ternary solutions with extremely low H_2SO_4 but high HNO_3 concentrations. Such mixtures occur under thermodynamic equilibrium conditions when the temperature drops below the frost point or alternatively under non-equilibrium conditions induced by gravity waves. Both candidates are expected to possibly play important roles in the formation of solid PSCs. As outlined in the previous chapter, binary HNO_3/H_2O bulk solutions cannot be supercooled to temperatures around the stratospheric frost point. Therefore it is of interest to determine how low the concentration in H_2SO_4 has to be to enhance freezing rates in ternary solutions. This has been discussed briefly by Meilinger *et al.*[23] In the following we evaluate these experiments in more detail. Several solutions with 48 wt % HNO_3 (fixed) and varying amounts of H_2SO_4 between 0 and 1.4 wt % have been prepared. The freezing points of these solutions are shown in Figure 17 (note that the x-axis is plotted logarithmically). While bulk solutions containing $0 \le H_2SO_4$ wt % ≤ 0.01 froze at high temperatures typical for binary HNO_3/H_2O solutions, the freezing temperatures of solutions with 0.1 and 1.4 wt % of H_2SO_4 were significantly lowered. To guide the eye, the solid line in Figure 17 shows the steep decrease in freezing temperature between 0.01 and 0.1 wt %. At first sight one might expect that the addition of a component (in this case H_2SO_4) to a solution reduces its freezing temperature. This is quite common and well-known in many systems. For example, adding H_2SO_4 or HNO_3 to water reduces the freezing temperature of ice by many kelvins. However, in these cases also the melting point of ice is lowered due to the second component, which leads to a smaller saturation ratio at the same temperature and therefore to a reduced freezing temperature. This is very different in the present case where freezing is quenched by very small H_2SO_4 amounts. Here, the saturation ratio, S_{NAT}, and the melting point temperature increase with enhanced H_2SO_4 concentrations, while the freezing temperature decreases. In Figure 17 the dashed lines give temperatures of constant S_{NAT} as a function of H_2SO_4 concentrations. The isosaturation temperature slightly increases with increasing H_2SO_4 concentration, since at the same temperature a solution containing 2 wt % H_2SO_4 is slightly more supersaturated than a binary HNO_3/H_2O solution (both with 48 wt % HNO_3). Comparing these lines with the measured freezing points shows that the solutions with no or 0.01 wt % H_2SO_4 usually froze when S_{NAT} is smaller than 10, while the ones with 0.1 and 1.4 wt % usually revealed a saturation ratio of 20 or more. Hence,

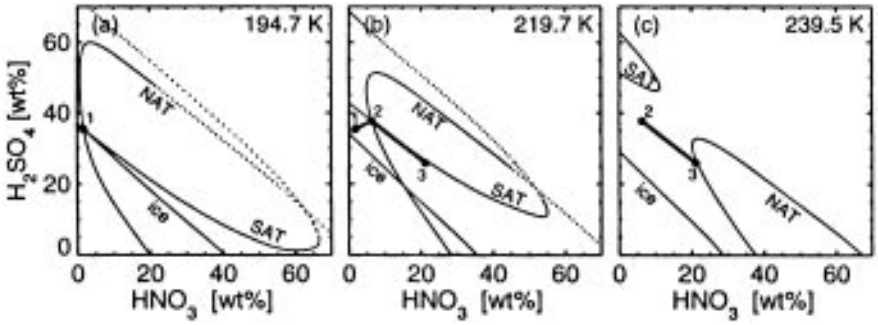

Figure 16. Phase diagrams of the ternary $H_2SO_4/HNO_3/H_2O$ system showing, as thin solid lines, the coexistence curves of NAT, SAT, and ice with the liquid for 194.7 (a), 219.7 (b), 239.5 K (c). The dotted part of the coexistence curves is outside the validity range of our model but is shown for clarity. Labels NAT, SAT, and ice are given on that side of the coexistence curves where the liquid is supersaturated with respect to the particular solid. Thick solid lines indicate the evolution of the sample from Figure 14 during melting. Points 1−3 mark several different eutectic and melting points. Point 1, NAT/SAT/ice triple eutectic point (194.7 K; ice melts); 1−2, the connected NAT/SAT/liquid coexistence points for this sample at temperatures between 194.7 and 219.7 K. 2, SAT is completely melted. 2−3, NAT/liquid coexistence points for this sample at temperatures between 219.7 and 239.5 K. 3, the remaining NAT is completely melted, and the sample is liquid at its initial composition.

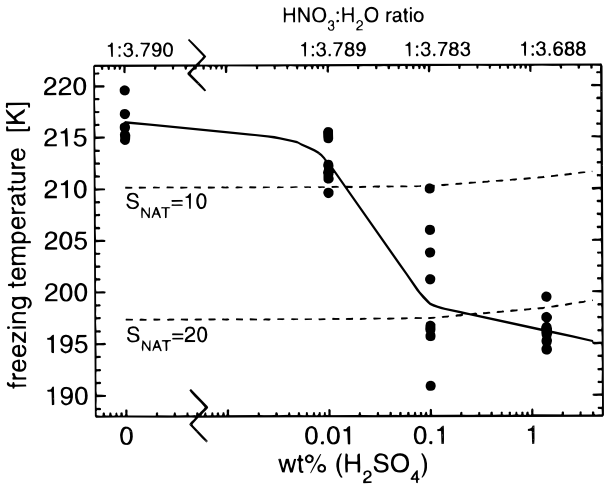

Figure 17. Freezing temperatures of ternary $HNO_3/H_2SO_4/H_2O$ solutions 1 cm^3 in volume as a function of H_2SO_4 concentration. The two dashed lines indicate the temperatures at which the supersaturation of the solutions with respect to NAT is 10 and 20; the solid line is just to guide the eye. Note that the *x*-axis is plotted logarithmically.

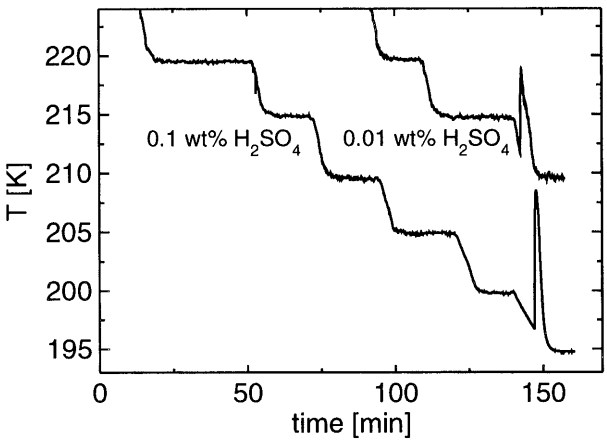

Figure 18. Freezing experiment of a $HNO_3/H_2SO_4/H_2O$ ternary solution showing the temperature evolution of the sample. Upper line, solution containing 48 wt % HNO_3 and 0.01 wt % H_2SO_4 freezing at a temperature of 211.6 K; lower line, the same solution after adding some solution enriched in H_2SO_4 so that the concentration was adjusted to 48 wt % HNO_3 and 0.1 wt % H_2SO_4. The freezing temperature is reduced by approximately 15 K to 196.7 K.

saturation ratios and freezing probabilities show an opposing behavior. The large scatter in the freezing points of the 0.1 wt % H_2SO_4 solution is possibly due to the uncertainties in the H_2SO_4 concentration, where quite small deviations lead to substantial changes in the freezing point. To exclude heterogeneous effects we performed experiments in the following manner: first a solution with 48 wt % HNO_3 and 0.01 wt % H_2SO_4 was prepared and cooled down to its freezing point twice. Then, a small amount of a solution equally concentrated in HNO_3 and more concentrated in H_2SO_4 was added to the original solution, so that the final composition was 48 wt % HNO_3 and 0.1 wt % H_2SO_4. This solution was then again cooled down to its freezing point. With this method we are sure that we can only enhance the chance of heterogeneous freezing, because of possibly adding more dust particles and increasing the surface area of the glass wall in contact with the solution. Also the total volume becomes slightly larger, which makes homogeneous nucleation more favorable. Some experimental results using this procedure are shown in Figure 18. While the freezing of the solution before the treatment occurred at 209.6 (not shown) and 211.6 K (upper curve), the freezing point afterward was decreased to 196.7 K (lower curve). The same behavior was found in another experiment with this procedure (211.0 and 212.3 K before, 190.9 afterward), strongly suggesting that the quenching of the freezing is indeed due to the small increase in H_2SO_4 concentration. Also note that the result is independent of whether the mole fraction or the weight fraction of HNO_3 is kept constant. The ratio of HNO_3:H_2O mole fraction at 48 wt % HNO_3 and 0 wt % H_2SO_4 is 1:3.790, while it is 1:3.783 for a solution with 48 wt % HNO_3 and 0.1 wt % H_2SO_4; this small change should not affect the nucleation process. We do not have a satisfactory explanation for the observed strong effect of small amounts of H_2SO_4 on the freezing points of ternary solutions, while its experimental significance is clearly evident.

In our earlier paper we have proposed that stratospheric aerosols in thermodynamic equilibrium will freeze below the frost point when ice is precipitating from the droplets.[21] To investigate this process in more detail, we have performed experiments with a solution of 2.5 wt % H_2SO_4 and 36.3 wt % HNO_3 (called solution "G" in ref 21), corresponding to the aerosol composition at 188 K, i.e. about 1 K below the stratospheric frost point (at 55 mbar, 5 ppmv H_2O). When ice was freezing from this solution, NAT or any other hydrate usually did not nucleate readily, even when lowering the temperature to 187 K. Although these solutions were supercooled with respect to NAT and NAD when in equilibrium with the precipitating ice and the ice surface was large (as can be judged easily by the slushy appearance of the sample), it took up to 120 min until NAT nucleated. This suggests that the heterogeneous nucleation rate of NAD, NAT, and NAP on ice from the liquid is small. In contrast, seeding a liquid sample by adding small ice crystals to the solution after exhaling or spraying small water droplets into the glass led to a fast crystallization of NAT in the liquid. In the latter case NAT or a metastable hydrate probably first nucleated heterogeneously from the gas phase on the small ice crystals while they were sedimenting. When the crystals reached the gas/liquid interface they seeded NAT and ice in the solution leading to their simultaneous rapid growth. This would imply that the heterogenous nucleation rate of NAT on ice from the gas phase is large, as was also suggested by Iraci *et al.*,[28] who found that NAT nucleation on SAT films did not occur at saturation ratios of $\approx$30 or even higher, while NAT nucleated readily when ice was present under otherwise identical conditions. Thus the diffusion activation energy seems to play an important role for the nucleation process of NAT on ice, because it is large in the liquid but practically absent in the gas phase and therefore leads to a much smaller nucleation rate from the liquid. On the other hand, flow tube studies[62] exposing ice surfaces to stratospheric HNO_3 partial pressures at 191.5 K suggested that a metastable hydrate, probably NAD, formed preferentially in the beginning and only transformed to NAT after a time delay. In contrast, at 200 K NAT did not form at all in these experiments. Whether in our experiment at 188 K NAT is formed initially or via NAD cannot be concluded.

While our measurements indicate that NAT nucleation on ice from the liquid under equilibrium conditions is too small to be of stratospheric relevance, further detailed analyses are needed to determine the exact rate coefficients for the nucleation of NAD, NAT, and NAP on ice from the gas phase. Applied to the stratosphere this would imply that the ice crystal forming in a ternary droplets has to grow to a size where it is no longer completely covered by the liquid until nitric acid hydrates nucleate. This could then also lead to freezing of the remaining sulfuric acid as SAT, SAH, or SAO. This mechanism strongly depends on the morphology of the crystallizing droplets.

There is a second possible mechanism which could lead to freezing of nitric acid hydrates when ice crystallizes from stratospheric droplets. The absence of a fast nitric acid hydrate nucleation after ice has formed in the ternary solution experiment described above also could have been due to the presence of H_2SO_4 in the liquid. In contrast, in aerosol experiments NAT was observed to form within minutes after the crystallization of ice in binary HNO_3/H_2O submicron droplets at temperatures between 175 and 185 K.[45] This again shows the strong dependence of nitric acid hydrate nucleation on the concentration of H_2SO_4 in the liquid. Applied to the stratosphere, this provides a pathway for the freezing of nitric acid in lee waves below the frost point: Due to fast cooling, smaller droplets would assume almost binary HNO_3/H_2O concentrations[23] and then freeze as NAT as soon as ice forms below the frost point.

4. Discussions and Conclusions

Research on the microphysics of polar stratospheric clouds (PSCs) currently focuses on the identification of chemical composition and formation processes of solid cloud particles. In particular the mechanisms leading to the freezing of solid acid hydrates are not well understood. There is little doubt about the freezing of solution droplets a few kelvins below the frost point leading to water ice formation, which possibly induces the precipitation of acid hydrates due to heterogeneous nucleation. However, it is presently unknown whether there is a mechanism of acid hydrate formation above the frost point.

The present work shows that homogeneous nucleation rates of binary or ternary solutions with thermodynamic equilibrium compositions above the frost point are much too low to be of importance for PSC freezing. The experiments are based on the freezing of bulk solutions and hence require the transfer of the measured rates from the laboratory situation ($V \simeq 1$ cm^3) to the stratospheric droplets ($V \lesssim 10^{-12}$ cm^3). This is achieved by showing that the freezing of these solutions is a stochastic process which enables Poisson statistics to be exploited and thereby to determine upper bounds of the freezing rates even when the number of observed freezing events is small or zero.

In contrast to previous work, it is shown that a single bulk experiment with no freezing event at all may be used to exclude homogeneous freezing of stratospheric droplets at a very high level of confidence. Hence, for very low nucleation rates a bulk phase experiment with large volume can easily yield more information than an aerosol droplet experiment, where to reach similar products of solution volume and total observation time (Vt_{tot}) would require times much too long for practical measurements in the laboratory.

The rate coefficients determined in this work represent upper bounds for homogeneous nucleation. However, since for the investigated binary and ternary solutions the upper bounds are not sufficient for droplet freezing under stratospheric conditions, the true homogeneous rates are even smaller.

Moreover, the measurements reveal that none of the substrates tested did enhance the freezing due to heterogeneous nucleation to an extent which affects the freezing probability of stratospheric aerosols in a significant way. In the bulk experiments no particular care was taken to deactivate the walls of the test tubes used for containment nor were the samples subjected to special filtering or other cleaning techniques. Other investigations specifically testing stratospherically important nuclei corroborate this conjecture.[54,55] Unless the stratosphere contains nuclei much better suited than those present in these laboratory experiments, heterogeneous nucleation does not seem to play a major role in the freezing of liquid aerosols.

The only care that has to be taken in the experiments to avoid artificial seeding of the solutions is to ensure sufficiently slow cooling. During rapid cooling, the hydrates may form directly from the vapor phase above the liquid either on the containment walls or in the form of small solid germs on foreign aerosol particles (e.g. on the ice crystals formed after exhaling into the test tube). When the solutions get into contact with these hydrates, rapid freezing follows.

The experiments furthermore show that once nucleation of an acid hydrate has occurred it grows rapidly and without evidence for a delay. From this we conclude that the formation of an activated but amorphous state at sufficiently low temperatures, as it has been recently suggested in the literature, is unlikely to exist.

The present experiments leave open two pathways for the formation of solid hydrates of nitric or sulfuric acid from liquid aerosols: Either the hydrates form heterogeneously on water ice below the frost point or they form above the frost point after homogeneous nucleation from binary or almost binary HNO_3/H_2O solutions whose H_2SO_4 concentrations due to strong temperature fluctuations have been reduced to values $\lesssim 0.01$ wt %. In both cases the bulk experiments indicated sufficiently fast nucleation rates.

However, in the cases where freezing appears to be possible also the limits of bulk experiments become evident: Firstly, high nucleation rates are not easily detectable because the nucleation occurs either directly after or even before reaching the desired temperature in a bulk, and secondly heterogeneous nucleation on the walls may now play a major role. This reveals the complementary character of bulk and aerosol freezing experiments. While most of the rate coefficients for homogeneous nucleation of equilibrium solutions are in a range that is detectable in bulk but not in aerosol freezing experiments ($J \lesssim 1/(Vt_{tot}) = 10^{-2}-10^{-5}$ cm^{-3} s^{-1}), the much smaller volumes and the contact-free suspension of aerosol experiments enables measurement of the much faster rates expected for nucleation processes in solutions under nonequilibrium or for sub-frost-point conditions. In the future, reliable measurements of this kind will help to clarify the open problems of PSC freezing.

Acknowledgment. We thank Keith Beyer, Mario Molina, Kyuil Ji, and Jean-Claude Petit for making their freezing data available to us and Renyi Zhang for providing some unpublished DSC data. Also thanks to Ken Carslaw and Tim Onasch for helpful comments and Laura Iraci, Ann Middlebrook, Azadeh Tabazadeh, and Renyi Zhang for sending us preprints of their work. Support from the BMBF (Grant for T.K. under Contract 01LO9506), the UBA (Grant No. 104 02 814 for B.P.L.), and the Friedrich-Ebert-Stiftung (Grant for U.M.B.) is gratefully acknowledged.

Appendix 1

(a) The Poisson Distribution. The binomial distribution of eq 1 reduces to the Poisson distribution of eq 2 when $m - k \gg 1$ and $p \ll 1$. In this case, the factorials can be expanded according to Stirling's formula $k! \simeq (2\pi k)^{1/2} k^k \, e^{-k}$. In the result p is expressed as $p = (k - \epsilon)/m$ and expansion to the first order in ϵ yields

$$\left(\frac{1-p}{m-k}\right)^{m-k} = m^{-m+k} \exp\left[(m-k)\ln\left(1+\frac{\epsilon}{m-k}\right)\right] \simeq m^{-m+k}\, e^{k-mp} \quad \text{(A1)}$$

from which eq 2 is easily derived.

(b) The Normal Distribution. The binomial distribution of eq 1 reduces to the normal distribution of eq 12 when $m - k \gg$

1 and $k \gg 1$. For $m - k \geq 50$ and $k \geq 50$, the factorials can be expanded according to Stirling's formula with an accuracy better than 0.17%. In the result p is expressed as $p = (k - \epsilon)/m$ and all terms are expanded to second order in ϵ, which leads to the expression[63]

$$\left(1 - \frac{\epsilon}{k}\right)^k \left(1 + \frac{\epsilon}{m-k}\right)^{m-k} = \exp\left[k \ln\left(1 - \frac{\epsilon}{k}\right) + (m-k)\ln\left(1 + \frac{\epsilon}{m-k}\right)\right] \simeq \exp\left[-\frac{\epsilon^2}{2}\left(\frac{1}{k} + \frac{1}{m-k}\right)\right] = \exp\left[-\frac{\epsilon^2}{2\sigma^2}\right] = \exp\left[-\frac{(k-mp)^2}{2\sigma^2}\right] \quad \text{(A2)}$$

From this eq 12 follows directly.

Appendix 2

The fiducial limits of ω for a normal distribution are defined in a manner very similar to eqs 10a,b for the Poisson distribution:

$$x = \frac{1}{\sigma(2\pi)^{1/2}} \int_{-\infty}^{n_{fr}-1} dk \exp\left(-\frac{(k - \omega_{low}t_{tot})^2}{2\sigma^2}\right) \quad \text{(A3)}$$

and

$$x = \frac{1}{\sigma(2\pi)^{1/2}} \int_{n_{fr}+1}^{\infty} dk \exp\left(-\frac{(k - \omega_{up}t_{tot})^2}{2\sigma^2}\right) \quad \text{(A4)}$$

Evaluation of these integrals in terms of the error function $\mathrm{erf}(x) = 2\pi^{-1/2} \int_0^x dt \exp(-t^2)$ leads to eqs 13a,b when $\sigma \simeq n_{fr}^{1/2}$ is used.

In Table 2 the upper and lower fiducial limits are given for selected numbers of freezing events, n_{fr}, at a confidence level of $x = 0.999$ as calculated using Poisson statistics. In Table 3 also the values of the normal distribution fiducial limits are given for $n_{fr} \geq 100$. Note that the normal distribution limits are not symmetrical to the Poisson distribution limits, as has been explained by Regener.[39] Table 4 provides some values for the inverse error function $\mathrm{erf}^{-1}(2x - 1)$ at typical confidence levels x.

TABLE 2: Upper and Lower Fiducial Limits for Selected Numbers of Nucleation Events, n_{nuc}, at a Confidence Level of $x = 0.999$[a] As Calculated Using Poisson Statistics

$\omega_{low}t_{tot}$	n_{nuc}	$\omega_{up}t_{tot}$
nd[b]	0	6.908
0.001	1	9.233
0.045	2	11.229
0.191	3	13.062
0.429	4	14.794
0.739	5	16.455
1.107	6	18.062
1.520	7	19.626
1.971	8	21.156
2.452	9	22.657
2.961	10	24.134
5.794	15	31.244
8.958	20	38.042
12.337	25	44.636
15.869	30	51.083
19.518	35	57.418
23.260	40	63.662
27.078	45	69.833
30.959	50	75.942
38.878	60	88.007
46.963	70	99.909
55.180	80	111.682
63.506	90	123.348
71.921	100	134.924
159.130	200	247.675
433.739	500	573.028

[a] The confidence level $x = 0.999$ is the probability that $\omega_{low} < \omega$ or that $\omega < \omega_{up}$. [b] nd, not defined.

TABLE 3: Upper and Lower Normal Distribution Fiducial Limits for Selected Numbers of Nucleation Events, n_{nuc}, at a Confidence Level of $x = 0.999$[a]

$\omega_{low}t_{tot}$	n_{nuc}	$\omega_{up}t_{tot}$
68.098	100	131.902
155.298	200	244.702
429.900	500	570.100

[a] The confidence level $x = 0.999$ is the probability that $\omega_{low} < \omega$ or that $\omega < \omega_{up}$.

TABLE 4: Values for the Inverse Error Function $\mathrm{erf}^{-1}(2x-1)$ at Selected Confidence Levels x

x	$\mathrm{erf}^{-1}(2x-1)$
0.900	0.906 19
0.950	1.163 09
0.990	1.644 98
0.999	2.185 12

References and Notes

(1) Carslaw, K. S.; Luo, B. P.; Clegg, S. L.; Peter, Th.; Brimblecombe, P; Crutzen, P. J. *Geophys. Res. Lett.* **1994**, *21*, 2479−2482.

(2) Tabazadeh, A.; Turco, R. P.; Drdla, K.; Jacobson, M. Z.; Toon, O. B. *Geophys. Res. Lett.* **1994**, *21*, 1619−1622.

(3) Drdla, K.; Tabazadeh, A.; Turco, R. P.; Jacobson, M. Z.; Dye, J. E.; Twohy, C.; Baumgardner, D.; Kelly, K. K.; Chan, R. P.; Loewenstein, M. *Geophys. Res. Lett.* **1994**, *21*, 2473−2478.

(4) Toon, O. B.; Browell, E. V.; Kinne, S.; Jordan, J. *Geophys. Res. Lett.* **1990**, *17*, 393−396.

(5) Beyerle, G.; Luo, B. P.; Neuber, R.; Peter, T.; McDermid, I. S., submitted to *J. Geophys. Res.*

(6) Dye, J. E.; Baumgardner, D.; Gandrud, B. W.; Kawa, S. R.; Kelly, K. K.; Loewenstein, M.; Ferry, G. V.; Chan, K. R.; Gary, B. L. *J. Geophys. Res.* **1992**, *97*, 8015−8034.

(7) Dye, J. E., Baumgardner, D.; Gandrud, B. W.; Drdla, K.; Barr, K.; Fahey, D. W.; Delnegro, L. A.; Tabazadeh, A.; Jonsson, H. H.; Wilson, J. C.; Loewenstein, M.; Podolske, J.; Chan, K. R. *Geophys. Res. Lett.* **1996**, *23*, 1913−1916.

(8) Poole, L. R.; McCormick, M. P. *J. Geophys. Res.* **1988**, *93*, 8423−8430.

(9) Crutzen, P. J.; Arnold, F. *Nature* **1986**, *324*, 651−655.

(10) Toon, O. B.; Hamill, P.; Turco, R. P.; Pinto, J. *Geophys. Res. Lett.* **1986**, *13*, 1284−1287.

(11) Hanson, D.; Mauersberger, K. *Geophys. Res. Lett.* **1988**, *15*, 855−858.

(12) Browell, E. V.; Butler, C. F.; Ismail, S.; Robinette, P. A.; Carter, A. F.; Higdon, N. S.; Toon, O. B.; Schoeberl, M. R.; Tuck, A. F. *Geophys. Res. Lett.* **1990**, *17*, 385−388.

(13) Beyerle, G.; Neuber, R.; Schrems, O.; Wittrock, F.; Knudsen, B. *Geophys. Res. Lett.* **1994**, *21*, 57−60.

(14) Rosen, J. M.; Kjome, N. T.; Oltmans, S. J. *J. Geophys. Res.* **1993**, *98*, 12741−12751.

(15) Molina, M. J.; Zhang, R.; Wooldridge, P. J.; McMahon, J. R.; Kim, J. E.; Chang, H. Y.; Beyer, K. D. *Science* **1993**, *261*, 1418−1423.

(16) Iraci, L. T.; Middlebrook, A. M.; Wilson, M. A.; Tolbert, M. A. *Geophys. Res. Lett.* **1994**, *21*, 867−870.

(17) Worsnop, D. R.; Fox, L. E.; Zahniser, M. S.; Wofsy, S. C. *Science* **1993**, *259*, 71−74.

(18) Marti, J.; Mauersberger, K. *J. Phys. Chem.* **1994**, *98*, 6897−6899.

(19) Fox, L. E., Worsnop, D. R.; Zahniser, M. S.; Wofsy, S. C. *Science* **1995**, *267*, 351−355.

(20) Tabazadeh, A.; Toon, O. B. *J. Geophys. Res.* **1996**, *101*, 9071−9078.

(21) Koop, T.; Biermann, U. M.; Raber, W.; Luo, B. P.; Crutzen, P. J.; Peter, Th. *Geophys. Res. Lett.* **1995**, *22*, 917−920.

(22) Tabazadeh, A.; Toon, O. B.; Hamill, P. *Geophys. Res. Lett.* **1995**, *22*, 1725−1728.

(23) Meilinger, S. K.; Koop, T.; Luo, B. P.; Huthwelker, T.; Carslaw, K. S.; Krieger, U.; Crutzen, P. J.; Peter, Th. *Geophys. Res. Lett.* **1995**, *22*, 3031−3034.

(24) Molina M. J. In *The Chemistry of the Atmosphere: The Impact of Global Change*; Calvert, J. G., Ed.; Blackwell Scientific Publishers: Oxford, U.K., 1994.
(25) Ravishankara, A. R; Hanson, D. R. *J. Geophys. Res.* **1996**, *101*, 3885−3890.
(26) Carslaw, K. S.; Peter, Th. In *Polar stratospheric ozone, Proceedings of the 3rd European workshop*, Schliersee, Germany, 1995; Pyle, J. A., Harris, N. R. P., Amanatidis, G. T., Eds.; European Commission Publication Office: Luxembourg, 1996.
(27) Hanson, D. R.; Ravishankara, A. R.; Solomon, S. *J. Geophys. Res.* **1994**, *99*, 3615−3629.
(28) Iraci, L. T.; Middlebrook, A. M.; Tolbert, M. A. *J. Geophys. Res.* **1995**, *100*, 20969−20977.
(29) Ohtake, T. *Tellus* **1993**, *45B*, 138−144.
(30) Beyer, K. D. Laboratory experiments of chemical reactions on PSC particles. Ph.D. Thesis, Massachusetts Institute of Technology, Cambridge, MA, 1994.
(31) Beyer, K. D.; Seago, S. W.; Chang, H. Y.; Molina, M. J. *Geophys. Res. Lett.* **1994**, *216*, 871−874.
(32) Song, N. *Geophys. Res. Lett.* **1994**, *21*, 2709−2712.
(33) Anthony, S. E.; Tisdale, R. T.; Disselkamp, R.; Tolbert, M. A.; Wilson, J. C. *Geophys. Res. Lett.* **1995**, *22*, 1105−1108.
(34) Disselkamp, R. S.; Anthony, S. E.; Prenni, A. J.; Onasch, T. B.; Tolbert, M. A. *J. Phys. Chem.* **1996**, *100*, 9127−9137.
(35) Bertram, A. K.; Patterson, D. D.; Sloan, J. J. *J. Phys. Chem.* **1996**, *100*, 2376−2383.
(36) Note that the probability p for a single molecule to become the center of a critical nucleus is proportional to the observation time t for $t \ll mp/\omega$ but saturates ($p \rightarrow 1$) for $t \gg mp/\omega$. The probability for no nucleation obeys the equation $d(1 - p)/dt = -(\omega/m)(1 - p)$ with the solution $1 - p = \exp(-\omega t/m)$, which resembles the decay law eq 4 for the entire sample.
(37) Barlow, T. W.; Haymet, A. D. J. *Rev. Sci. Instrum.* **1995**, *66*, 2996−3007.
(38) Pruppacher, H. R.; Klett, J. D. *Microphysics of Clouds and Precipitation*; D. Reidel Publishing Co.: Dordrecht, Holland, 1978.
(39) See also: Regener, V. H. *Phys. Rev.* **1951**, *84*, 161−162. Brandt, S. *Datenanalyse*, 3rd ed.; BI-Wissenschaftsverlag: Mannheim, 1992.
(40) Larsen, N.; Knudsen, B. M.; Rosen, J. M.; Kjome, N. T.; Kyro, E. *Geophys. Res. Lett.* **1996**, *23*, 1091−1094.
(41) Ha, A.; Cohen, I.; Zhao, X.; Lee, M.; Kivelson, D. *J. Phys. Chem.* **1996**, *100*, 1−4.
(42) A glass point is the temperature at which a liquid turns into a glass upon cooling as evidenced by changes in its thermodynamic properties (i.e. molar volume, enthalpy, entropy, heat capacity, viscosity etc.). Strictly speaking, the glass point depends on the cooling rate applied to the system; however, for our purpose it is sufficient to think of it as being one single temperature which depends only on concentration.
(43) Cohen, I.; Ha, A.; Zhao, X.; Lee, M.; Fischer, T.; Strouse, M. J.; Kivelson, D. *J. Phys. Chem.* **1996**, *100*, 8518−8526.
(44) Johari, G. P.; Hallbrucker, A.; Mayer, E. *Science* **1996**, *273*, 90−92.
(45) Barton, N., Rowland, B.; Devlin, J. P. *J. Phys. Chem.* **1993**, *97*, 5848−5851.
(46) Tolbert, M. A.; Koehler, B. G.; Middlebrook, A. M. *Spectrochim. Acta* **1992**, *48A*, 1303−1313.
(47) Tang, I. N.; Fung, K. H.; Imre, D. G.; Munkelwitz, H. R. *Aerosol Sci. Technol.* **1995**, *23*, 443−453.
(48) Tang, I. N.; Munkelwitz, H. R. *Atmos. Environ.* **1993**, *27A*, 467−473.
(49) Luo, B. P.; Carslaw, K. S.; Peter, Th.; Clegg, S. *Geophys. Res. Lett.* **1995**, *22*, 247−250.
(50) Gable, C. M.; Betz, H. F.; Maron, S. H. *J. Am. Chem. Soc.* **1950**, *72*, 1445−1448.
(51) Mootz, D.; Merschenz-Quack, A. *Z. Naturforsch.* **1987**, *42b*, 1231−1236.
(52) Wood, G. R.; Walton, A. G. *J. Appl. Phys.* **1970**, *41*, 3027−3036.
(53) Middlebrook, A. M.; Iraci, L. T.; McNeill, L. S.; Koehler, B. G.; Wilson, M. A.; Saastad, O. W.; Tolbert, M. A.; Hanson, D. R. *J. Geophys. Res.* **1993**, *98*, 20473−20481.
(54) Biermann, U. M.; Presper, T.; Koop, T.; Mössinger, J.; Crutzen, P. J.; Peter, Th. *Geophys. Res. Lett.* **1996**, *23*, 1693−1696.
(55) Kärcher, B.; Peter, Th.; Biermann, U. M.; Schumann, U. J. *Atmos. Sci.* **1996**, *53*, 3066−3083.
(56) Luo, B. P.; Peter, Th.; Crutzen, P. *Geophys. Res. Lett.* **1994**, *21*, 1447−1450.
(57) Schäfer, K. In *Landolt-Börnstein Serie, II. Band, 5. Teil*; Springer Verlag: Heidelberg, 1969.
(58) Williams, L. R.; Golden, D. M. *Geophys. Res. Lett.* **1993**, *20*, 2227−2230.
(59) Williams, L. R.; Long, F. S. *J. Phys. Chem.* **1995**, *99*, 3745−3751.
(60) The experiment with 53.8 wt % HNO_3 shown in Figure 6 is not subject to such a procedure. It does not suffer from unintended seeding because of the high temperature (226 K).
(61) The slope is calculated from $(dw_n/dw_s = [w_n^0(1 + 3M_w/M_n) - 1]/[w_s^0(1 + 3M_w/M_n)])$. Here, w_n and w_s are the weight fractions of HNO_3 and H_2SO_4, respectively, w_n^0 and w_s^0 are the initial weight fractions of the solution, and M_w and M_n are the molar masses of H_2O and HNO_3, respectively.
(62) Hanson, D. R. *Geophys. Res. Lett.* **1992**, *19*, 2063−2066.
(63) The approximation in eq A2 requires $|\epsilon| \ll k$ and $|\epsilon| \ll m - k$. This is satisfied for all relevant values of k and x.
(64) Vuillard, G. *Bull. Soc. Chim.* **1954**, 802−807.
(65) Ji, K. Etudes de la compositions des aerosols stratosphériques polaires au moyen des diagrammes de phase stables, metastables et cinétiques des systems: HNO_3/H_2O , HCl/H_2O et H_2SO_4/H_2O. Ph.D. Thesis, L'université de Paris, Paris, 1994.
(66) Zhang, R., Laboratory investigations of heterogeneous chemistry important to ozone depletion in the stratosphere. Ph.D. Thesis, Massachusetts Institute of Technology, Cambridge, MA, 1993.
(67) Küster, F. W.; Kremann, R. *Z. Anorg. Chem.* **1904**, *41*, 1−42.
(68) Satoh, K.; Kanno, H. *Bull. Chem. Soc. Jpn.* **1982**, *55*, 1645−1646.